# FINITE ELEMENT MODELING OF DRILLING AZ91 MAGNESIUM FOAM REINFORCED WITH HOLLOW ALUMINA MICROSPHERES

by

Abdalla Mohammed

A Thesis presented to the faculty of the
American University of Sharjah
College of Engineering
In Partial Fulfillment
of the Requirements

for the Degree of Master of Science in
Mechanical Engineering

Sharjah, United Arab Emirates

July 2021

**Declaration of Authorship**

I declare that this thesis is my own work and, to the best of my knowledge and belief, it does not contain material published or written by a third party, except where permission has been obtained and/or appropriately cited through full and accurate referencing.

Signed…….

Date……02/07/2021…….

**Approval Signatures**

We, the undersigned, approve the Master's Thesis of Abdalla Mohammed

Title: Finite Element Modeling of Drilling AZ91 Magnesium Foam Reinforced with Hollow Alumina Microspheres

Date of Defense: 12-Jul-2021

| **Name, Title and Affiliation** | **Signature** |
|---|---|
| Dr. Sathish Kannan<br>Assistant Professor, Department of Mechanical Engineering<br>Thesis Advisor | |
| Dr. Wael Abuzaid<br>Associate Professor, Department of Mechanical Engineering<br>Thesis Committee Member | |
| Dr. Rajiv Selvam<br>Associate Professor, Department of Mechanical Engineering<br>Manipal Academy of Higher Education, Dubai Campus<br>Thesis Committee Member | |
| Dr. Mamoun Abdel-Hafez<br>Head<br>Department of Mechanical Engineering | |
| Dr. Lotfi Romdhane<br>Associate Dean for Graduate Affairs and Research<br>College of Engineering | |
| Dr. Sameer Al-Asheh<br>Interim Dean<br>College of Engineering | |
| Dr. Mohamed El-Tarhuni<br>Vice Provost for Research and Graduate Studies<br>Office Graduate Studies | |

## Abstract

Novel AZ91 magnesium syntactic foams are a potential choice for temporary biomedical implants. In many cases, holes of various sizes need to be machined on the biomedical implants using the drilling process to facilitate placement of implants inside the human body. In this study, the drilling performance of AZ91-magnesium foam is investigated under different lubrication methods such as dry, wet (Almag® mineral Oil), and cryogenic cooling. Drilling experiments were carried out using titanium aluminium nitride (TiAlN) physical vapor deposition (PVD) coated and uncoated twist drills on varying volume fractions of AZ91 magnesium syntactic foams (5%, 10%, and 15%) reinforced with hollow alumina microspheres. Test results showed a 30%-60% higher thrust forces generated with cryogenic machining compared to dry and wet machining while cutting AZ91-15% hollow alumina foam. This phenomenon shows the influence of alumina hollow microspheres on controlling the plastic deformation of the AZ91 magnesium matrix through effective work hardening and characteristic load transfer. Scanning electron microscope (SEM) investigation of cryogenic machined bore surfaces showed minimal drilling-induced surface defects. Based on the analysis carried out, cryogenic machining is recommended as a sustainable drilling process for AZ91-magnesium syntactic foams. A three-dimensional, thermo-mechanical finite element-based model for drilling magnesium syntactic foam using AdvantEdge$^{TM}$ is presented for different lubrication conditions. Metal cutting tests are performed and comparison with predicted data is provided. The predicted machining induced stress from the finite element model showed a compressive stress in case of cryogenic cooling compared to dry machining which will give a better surface integrity and quality to the machined surface and will reduce the danger of crack propagation and crack growth. Based on the analysis carried out, cryogenic machining is recommended as a sustainable drilling process for AZ91-magnesium syntactic foams



**Keywords:** ***Hole making; Surface integrity; Machining forces; AZ91 magnesium; Metal foam; AdvantEdge$^{TM}$.***

## Table of Contents

Abstract…… .....4
List of Figures .....7
List of Table .....9
Chapter 1. Introduction .....10
1.1 Overview .....10
1.2 Thesis Objectives: .....12
Chapter 2. Background to Metal Syntactic Foams .....13
2.1 Introduction .....13
2.2 Metal Matrix Syntactic Foams .....13
2.3 Literature Review .....13
2.3.1 Machining of syntactic foams…….....13
2.3.2 Machining induced stress…… .....16
Chapter 3. Experiment and Finite Element Modelling Methodology.....19
3.1. Twist Drills.....19
3.2. Drilling and Lubrication Conditions .....20
3.3. Machining Force, Surface Roughness, Burr Formation, and Chip Morpholog 21
3.4 Finite Element Simulation.....22
3.4.1 Material model…….....23
3.4.2 Friction model…….....24
3.4.3 Boundary conditions……...24
3.4.4 Simulation methods…… ....25
3.5 Machining Induced Stress Measurements.....25
3.6 Damage Mechanism.....26
Chapter 4. Results and Discussion.....28
4.1. Drilling Thrust Force.....28
4.2 Surface Quality and Integrity .....34
4.3 Machining Induced Stress .....39
4.3.1 Effect of cutting speed……....40
4.3.2 Effect of feed rate…… .....41
4.3.3 Effect of microsphere volume fraction…….....42

4.3.4 Effect of tool coating…….. .....43
4.3.5 Effect of coolant type……. .....45
4.4 Drilling Burr Formation .....46
4.5 Chip Morphology .....49
4.6 Damage Mechanics .....52
4.6.1 Unit cell damage model…….....52
4.6.2 Effect of microsphere size and microsphere wall thickness…….....52
Chapter 5. Conclusions .....54
References ……...55
Vita…….....61

## List of Figures

Figure 2. 1 Effect of cutting speed on Ra Values ..... 15
Figure 2. 2 Axial Residual stress measured from the machined surface ..... 17
Figure 3. 1 Kennametal™ twist drills ..... 19
Figure 3. 2 a) Machine tool, b) drilling process and c) measured drilling force trace. 22
Figure 3. 3 Tool and workpiece mesh settings ..... 25
Figure 3. 4 Machining induced stresses along radial, axial, and hoop directions, respectively. ..... 26
Figure 3. 5 Unit cell model, tool, AZ91 matrix and Alumina hollow microsphere orientation ..... 26
Figure 3. 6 Meshing parameters for Unit Cell model ..... 27
Figure 4. 1 Effect of process parameters during machining AZ91-15% magnesium foam; (a) effect of cutting speed, and (b) effect of feed in mm/rev. ..... 29
Figure 4. 2 Effect of alumina volume fraction on thrust force during machining AZ91-magnesium foam. ..... 31
Figure 4. 3 Effect of a) type of coolant and b) tool coating on thrust force during machining of AZ91-15% magnesium foam. ..... 33
Figure 4. 4 Effect of process parameters a) cutting speed and b) feed on machined bore surface roughness (Ra) during machining of AZ91-15% syntactic foam. 35
Figure 4. 5 Effect of coolant on machined bore surface roughness (Ra) during machining of AZ91-15% alumina syntactic foam. ..... 37
Figure 4. 6 Some of the commonly found drilling induced defects during machining of AZ91 magnesium-alumina syntactic foam ..... 38
Figure 4. 7 a) Effect of hollow alumina volume fraction on bore surface roughness. 39
Figure 4. 8 Effect of cutting speed on the machining induced stress. ..... 40
Figure 4. 9 Effect of feed rate on the machining induced stress. ..... 42
Figure 4. 10 Effect of Volume fraction on the machining induced stress ..... 43
Figure 4. 11 Effect of tool coating on the machining induced stress ..... 44
Figure 4. 12 Effect of lubrication method on the machining induced stress ..... 45
Figure 4. 13 Effect of coolant on burr height. ..... 46
Figure 4. 14 Different types of edges produced at the hole exit side of the AZ91-15%magnesium foam. ..... 47
Figure 4. 15 Effect of alumina volume fraction on burr height during machining AZ91-magnesium syntactic foam under dry conditions; (a) Entry burr height and (b) exit burr height. ..... 49

Figure 4. 16 Chip morphology of AZ91-15% magnesium foam a) wet machining b) dry machining c) representative tool wear. ..... 51

Figure 4. 17 microsphere of 2 mm diameter and 0.1 mm wall thickness ..... 52

Figure 4. 18 Thrust force variation with a) microsphere diameter and b) microsphere wall thickness. ..... 53

## List of Table

Table 3. 1 Chemical composition of the hollow alumina reinforcement (supplier data) .....19
Table 3. 2 Properties of Kennametal™ drill tools (manufacturer data).....20
Table 3. 3 Test factors.....21
Table 3. 4 Johnson cook Parameters [19].....24
Table 4. 1 AZ91 with hollow alumina drilling parameters.....34
Table 4. 2 Unit cell damage model parameters.....52

# Chapter 1. Introduction

## 1.1 Overview

A composite material is a system of materials composed of two or more materials, which are not soluble to each other on a standard scale. Take the example for concrete, which has a combination of cement, sand, stones, and water. If microscopic composition (molecular level) happens, then the material is known as an alloy for metals. Normally, composite materials consist of two phases.[1] One phase is called the matrix phase and the other is the reinforcement phase. The matrix holds the reinforcement to obtain the desired mechanical properties of the new material. In fact, composite material shows an improved strength which is superior to that of matrix and reinforcement alone.

Composites are light in weight in comparison to wood and steel. Their lightness is crucial for increasing fuel efficiency involved automobiles and aeroplanes. Composites can be manufactured to be stronger compared to Aluminum or steel. When a metal is having uniform strength in all directions, composites can be stronger in one direction. Some materials may be strong and heavy, whereas others can be weak and light. Composites can be tailored to both strong as well as light. This particular property is the reason behind this material to be used in the aeroplane. In today's world, we can see that among all the structures, the one made up of composite has a high strength to weight ratio [2]. Composites resist corrosion which occurs from weather and particularly harsh chemicals that consume other materials. They are an excellent choice for storage of chemicals. In outdoor conditions, they can withstand harsh climate and wide changes in temperature. Composites can absorb high impulse energy like the force of a bullet, or the blasts coming from explosions. Because of this reason, it is used in making bulletproof vests and panels. Because of composite's design flexibility, designers have the freedom to create any shape like whether it is simple or complex. The surface of the composites can also be designed to any finish or texture, from smooth to rough. Composites can obtain a near-net shape. Thus, less amount of finishing work is needed. Composites last longer compared to other materials. So, they require very little maintenance. They also have low thermal conductivity. Based on the matrix phase, composites can be classified into three types: (a) Polymer Matrix Composites (PMCs), (b) Metal Matrix Composites (MMCs) and (c) Ceramic Matrix Composites (CMCs).[1]

Among these composites, metal matrix composites are commonly used in many applications in the industry due to their amazing strength and wear resistance. A notable example is the cylinder liners used in internal combustion engines. The excellent wear resistance in MMC materials is due to the reinforcements of hard abrasive ceramics present in the matrix.[3]

Two of the most notable metal matrix composites used in certain industries are aluminum matrix composites and magnesium matrix composites. Magnesium matrix composite is another potential composite which is used in aerospace and defense applications. This is owing to their low density in addition to good mechanical and physical properties [4]. When compared to SiC reinforced Al MMCs, the magnesium MMC reinforced with SiC gives better creep and wear resistance. Al2O3 reinforcement helps to improve wettability and bonding strength of aluminum metal matrix composites. If we increase the percentage composition of reinforcements, we can increase the density, hardness, and ultimate tensile strength [5].

Syntactic foam is a binary material which basically consists of preformed hollow microspheres and a matrix, which binds them, to get the required strength and stiffness at a reduced weight when compared to monolithic materials . The characteristics of microspheres and the matrices will directly affect the thermal, electrical as well as mechanical characteristics of syntactic foams. Studies show that 65% is the highest volume percentage of microspheres that can be attained in MMSF. Due to hollow microspheres, the foam has 50% porosity, which helps to save weight compared to conventional materials.

Use of syntactic foams benefits from lower fuel consumption and increase in payload capacity. Syntactic foams can be used to tailor the composition based on our interests. Syntactic foams are used in marine applications due to low moisture absorption and buoyancy. They can also be used in insulation of deep-water pipes, hulls of the boat and soccer balls.

Based on the cellular structure, syntactic foams can be classified into two types: (a) open-cell and (b) closed cell [6]. In this thesis, focus will be on closed-cell syntactic foam [7]. In normal cases, closed-cell foams will have more density and strength in comparison to open-cell foams.

## 1.2 Thesis Objectives:

1. Investigate the performance of sustainable cooling methods during hole drilling of AZ91 magnesium metal syntactic foams reinforced with hollow alumina microspheres.
2. Study the effect of microsphere size, cutting parameters and tool coating during drilling process of AZ91 syntactic foams.
3. To develop three-dimensional Finite element model to simulate thrust force generated during machining AZ91 magnesium reinforced with hollow alumina microspheres.
4. Study the influence of hollow alumina reinforcement on chip formation during drilling process.
5. Identify the various failure mechanisms contributing to chip formation.
6. Study machining induced stress variation with coolant method as well as microsphere size and thickness effects on drilling thrust force.
7. Investigate Damage model of the hollow microsphere using unit cell model and predict machining forces and average interfacial stresses via FEM.

# Chapter 2. Background to Metal Syntactic Foams

## 2.1 Introduction

This chapter will provide a brief explanation of the literature with regards to metal matrix syntactic foams, its physical and mechanical properties, the constitutive models, and force models for the syntactic foams. As there are closed cell and open cell types of syntactic foams.

## 2.2 Metal Matrix Syntactic Foams

Metal syntactic foams have a higher stiffness to weight ratio and a reversible seemingly elastic region. Due to this, they are applicable for use in light structures. However, when compared to the base metal, other mechanical properties of the metal foams are quite inferior. So, they are limited to applications where strength is not the primary design criteria. To overcome this difficulty, a novel method of adding porosity was developed. This method is the usage of hollow microspheres as fillers. The surrounding porosity inside these stiff and strong microspheres, which are inside a metal matrix, leads to a material where we can achieve higher modulus and strength than that of the homogenous metals. This new material or composite is called metal matrix syntactic foam. In addition to weight reduction, control of the size porosity of the spherical shape of the microspheres helps in attaining high energy absorption under compression.

Rohatgi et al. [8] defined metal matrix syntactic foams as a unique type of composite which includes void microspheres present inside a matrix, such that the encircling porous zone, which is inside the thin shell of the microsphere leads to low density without a huge dip in mechanical properties. When compressing these syntactic foams, a large plateau region appears in the stress-strain graph. The size of this plateau can be adjusted by controlling thickness of the wall of the microsphere, volume fraction and average size of the microspheres and the total energy of microspheres that can be absorbed from compression.

## 2.3 Literature Review

**2.3.1 Machining of syntactic foams.** AZ91 magnesium-based closed-cell alumina syntactic foams are found to be potential materials to be used on key components used in aerospace, biomedical, automotive, and marine applications [9][10][11]. Magnesium

based metal composites are classified as difficult-to-cut due to their heterogeneous microstructure and inherent brittleness of the reinforcing ceramic phase [12][13][14]. Key challenges faced during machining of magnesium-based syntactic foams are dimensional accuracy due to edge delamination and surface disintegration [12, 13]. Besides, the formation of built-up-edge, machining induced defects primarily due to fracture of hollow ceramic microsphere poses severe surface integrity issues [13]. Past studies have shown a strong correlation between machined surface integrity and its influence on corrosion performance during machining magnesium alloys [15][16][17]. Machining with large radii cutting tools under liquid nitrogen cooling medium shows a positive impact on the sub-surface integrity of magnesium alloys [18][19][20]. Experimental studies on an AZ31B-O magnesium alloy using a cryogenic cooling method reported higher sub-surface compressive machining induced stress with reduced thickness of the deformed layer [9]. In another cutting test on AZ31 magnesium alloy using a dipped cryogenic drilling method, Ugur et al. [21] reported an increase in thrust force compared to dry machining. However, cryogenic machining is shown to produce smaller chips with lower adhesion.

During machining magnesium composite (AZ91D/5%Gr), the presence of graphite reinforcement has been cited as a useful medium to provide lubrication that reduces the surface roughness [22]. Drilling feed rate is found to be a dominant factor in controlling machined surface roughness. The higher the feed rate, the more severe is the surface anomalies with grooves and cracks caused due to strain hardening of the magnesium matrix material [23]. During micro-drilling of magnesium-silica nanocomposites, the chip morphology changed from short spiral type to powder type [24]. Surface quality reduced with higher values of volume fraction, feed rate with larger burrs formed [24]. In a study on machining magnesium-based metal composites, the chip morphology is found to be more dependent on the machining speed [14].

Sustainable machining processes such as dry machining, minimum quantity lubrication, and cryogenic cooling are key technologies worthwhile investigating for magnesium composite foams. During cryogenic drilling of AZ31B magnesium alloy, an increase in machined surface hardness is noted [25][26]. On the other hand, the minimum quantity lubrication (MQL) is shown to produce stable thrust force during

cutting AM60 Mg alloy. MQL method generates acceptable surface quality with the formation of discontinuous chips [27]. Berzosa et al. [28] developed a model to predict the machined surface roughness during the MQL drilling of magnesium UNSM11917 material. A point angle of 118 °is reported to produce better surface finish at high cutting speed under MQL conditions. During end milling of AZ91D magnesium alloy Ireneusz and Jarosław [29] investigated the roughness parameters to describe the effect of dry milling on the lateral and end face of these alloys. The Ra values recorded were between 0.58 to 0.75 µm in the lateral surface while on the end surface the values did not exceed 0.4 µm as shown in the Figure 2.1.

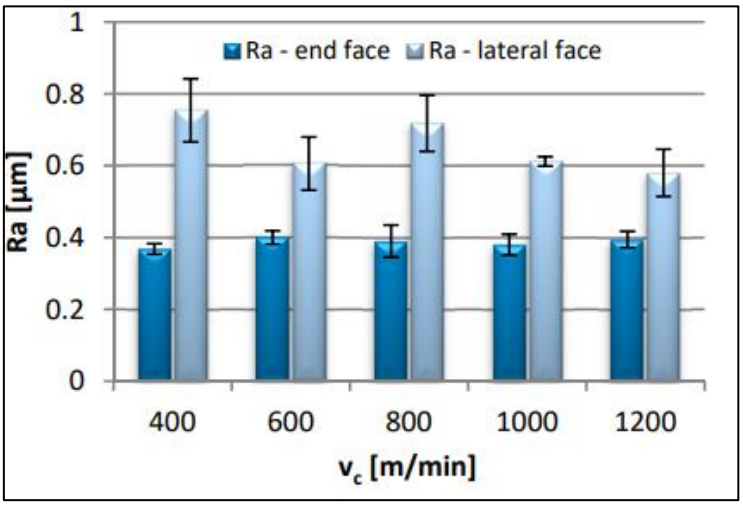


Figure 2.1 Effect of cutting speed on Ra Values [29]

Dry machining of magnesium alloys leads to poor surface finish, and material adhesion to the cutting tool results in surface smearing and reduction in tool life [30]. This is particularly important during drilling operations, which could lead to the poor evacuation of chips from the drilled hole. On the other hand, dry machining can also be beneficial from the environment perspective, provided the process parameters are optimized. There is a need to limit the cutting speed to prevent adhesion of soft magnesium on the tool flank face [31][32]. During dry drilling of AZ91 magnesium alloy, Wang et al. [33] developed wear mechanisms map in which they identified five different zones of tool wear mechanism. Bhowmick et al. [27] conducted drilling experiments on as-cast AZ91 magnesium alloy under dry and (H2O-MQL) conditions using non-hydrogenated diamond-like carbon (NH-DLC) coated HSS drills. Rapid tool

wear due to adhesion of soft magnesium resulted during dry drilling. On the other hand, drilling under (H2O-MQL) conditions improved tool life with decreased torque and cutting temperature to levels comparable to the flood cooling method. Drilling tests conducted on AM60 magnesium alloy using (H2O-MQL) and a fatty acid-based MQL showed a reduction of thrust forces, cutting temperature, and better surface finish [34].

Chen et al.[35] investigated the tool properties, tool geometry and machining parameters on the porous tungsten surface porosity. Another study by schoop et al. [36] obtained a suitable porous surface by controlling tungsten brittle microfracture. Heidari et al. [37] showed nanometer-level surface flatness possibility with open pores. Pusavec [38] used a multi-objective optimization mode via generic algorithm for cryogenic machining of cutting porous titanium to achieve the best machining performance by predicting the optimal input cutting parameters.

**2.3.2 Machining induced stress**. The processing and manufacturing of metallic component is often followed by an inhomogeneous thermal heat input which leads to machining induced stress formation. The magnitude and distribution of machining induced stresses play an important role for the proper design of the part and its manufacturing processes, as machining induced stress can have either positive or negative impact on the load bearing capabilities [39]. There are various methods to measure machining induced stress, some of them are destructive while others are non-destructive [40]. For destructive method, they are based on measuring the workpiece surface deformation after material removal. While for the later method, the amount of machining induced stress is estimated via the distortion of the crystal structure using diffraction methods. Recent work by Shan et al. [41] predicted machining induced stress in orthogonal cutting of Ti-6Al4V.Recent (2019) work by Wang et al. [42] and Yang and Zhou [43] in milling of complex surfaces and flank milling, respectively. A 3D analytical model of machining induced stresses has been developed. Numerical methodologies have become dominant over the last two decades, throughout the international community of modeling and machining operations, this includes the modeling of surface integrity [44][45]. FEA offers the ability to monitor complex surface integrity phenomena, such as phase transformations and dynamic recrystallization, makes them particularly good choice for the study of such complex

phenomena. However, FEM models are highly sensitive to the input data, most notably flow stress and friction, which are often not known with sufficient certainty. For instance, Umbrello et al. [46] studied the prediction of machining induced stress in AISI 316L using FEM to investigate the influence of constitutive model parameters on the results, noting that outputs were highly sensitive to material model parameters. To date, most modern FEM models focus primarily on cutting and thrust forces prediction as well as chip formation, without relatively little regard to the integrity of the machined surface [22][47]. Peron et al. [48] studied the residual stress generated in drilling AZ31 alloy using cryogenic cooling, they investigated the axial residual stress generated from the machined surface and concluded that totally compressive stresses were generated in case of cryogenic machining while for dry machining tensile stresses were found. The recorder values were 270 MPa "Tensile" and 143 MPa "compressive" in case of dry and cryogenic conditions respectively as shown in Figure 2.2.

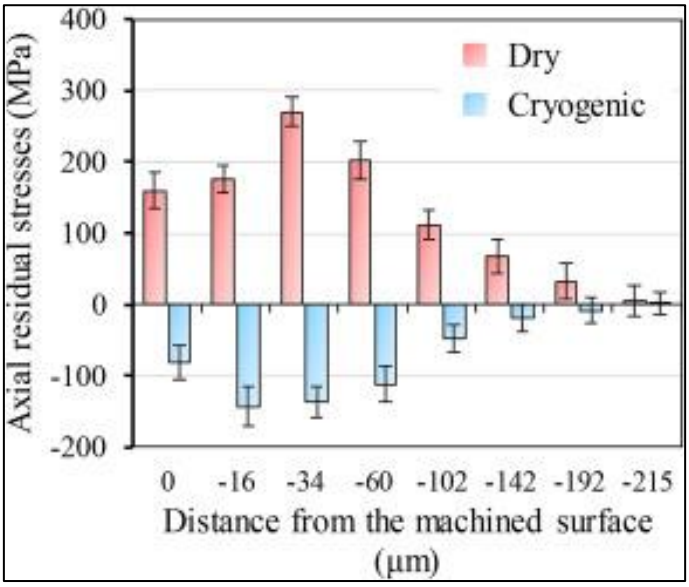


Figure 2.2 Axial Residual stress measured from the machined surface [48]

In this research FEM was implemented to predict the machining induced stress in the radial, axial, and hoop directions respectively, to investigate the process parameters and model parameters effect on the machined surface of the workpiece in order to have a clear vision of surface quality and integrity produced under various conditions and cooling methods.

A review of the literature shows a dearth of information on cryogenic drilling characteristics of magnesium-based metal matrix composites and their foams. The development of sustainable cooling methods for machining magnesium-based composites is critical from the perspective of mass production. This research investigates the performance of sustainable cooling methods during hole drilling of AZ91 magnesium metal syntactic foams reinforced with hollow alumina microspheres. The literature available till today concentrated mostly on statistical analysis and experimental investigation of various parameters during foam drilling operation. In this research, an attempt has been made to develop a three-dimensional, thermomechanical finite element simulation for modelling the drilling forces generated and stress generated in the surface during machining AZ91-hollow alumina syntactic foam.

## Chapter 3. Experiment and Finite Element Modelling Methodology

AZ91 magnesium syntactic foams reinforced with varying volume fractions of hollow alumina microspheres were manufactured via the stir-squeeze casting method. The melt was stirred at 500 rpm for 10 mins while the alumina microspheres were added. The melt temperature was set at 750°C with the mold preheated to 300°C under inert ultra-high purity argon gas at 3 liters per minute. The electromagnetic vibrator was used at 300 Hz to disperse the ceramic reinforcements, which were preheated to 200° C into the melt. The squeezing pressure was 117 MPa, which produced a billet of 50 mm diameter and 200 mm long. Cylindrical billets were manufactured by SWAM Equip Ltd, Chennai, India. The chemical composition of hollow alumina was obtained from the supplier (Pacific Rundum Co., Ltd, Tokyo, Japan).

Table 3. 1 Chemical composition of the hollow alumina reinforcement (supplier data)

| Avg microsphere size (mm) | Al203 | Fe203 | CaO | SiO2 | Na2O | Bulk density (g/cm3) |
|---|---|---|---|---|---|---|
| 0.3mm, 0.6mm | 99.7 | 0.006 | 0.013 | 0.026 | 0.27 | 1.700 |

### 3.1. Twist Drills

Two grades of carbide twist drills were used in this study. A multilayer titanium aluminium nitride (TiAlN) coated carbide drill, and uncoated K10 carbide drills were procured from Kennametal™. The twist drills were coated with TiAlN for superior wear and heat resistance using the physical vapor deposition method. Both the twist drills were φ5 mm in diameter. Properties of the twist drills used in this study are shown in Table 3.2.

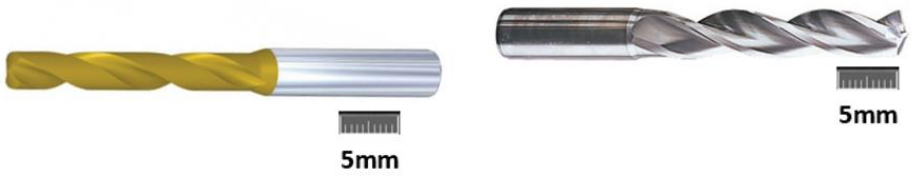


Figure 3. 1 Kennametal™ twist drills a.) TiAlN PVD coated b.) K10 uncoated carbide

Table 3. 2 Properties of Kennametal™ drill tools (manufacturer data)

| Property | TiAlN-PVD Coated | Uncoated |
|---|---|---|
| Flutes | 3 | 3 |
| Shank type | Straight | Straight |
| Drill diameter (mm) | 5 | 5 |
| Shank diameter (mm) | 6 | 6 |
| Grade | TiAlN Multilayer fine grain grade: KC7325 | Solid carbide K10 |
| Point angle | 140° | 140° |
| Helix angle | 30° | 30° |
| Flute length (mm) | 20 | 35 |

### 3.2. Drilling and Lubrication Conditions

Drilling experiments were carried out using a Doosan DNM-4500 3-axis milling machine as indicated in Figure 3.2. To investigate the effect of the lubrication method, three types of sustainable cooling methods were employed. Machining induced surface defects were characterized while cutting under dry, liquid nitrogen cryogenic and mineral oil-based coolant plunge drilling conditions. Machining conditions experimented under the range of machining speeds and feed rates are shown in Table 3.3. 5mm deep holes were drilled on magnesium syntactic foam samples reinforced with 5%, 10%, and 15% volume fraction of hollow aluminium oxide microspheres. Average values of machining force, surface roughness, and burr heights were recorded based on three holes drilled. Chip morphology was investigated under a Tescan scanning electron microscope. The functional performance of biodegradable AZ91 magnesium foams considered for advanced engineering applications requires exceptional surface quality and integrity requirements. The condition of the machined surface also controls the corrosion performance of the manufactured products [18]. This demands the need to employ favorable lubrication conditions to meet this requirement. As part of sustainable manufacturing, dry machining helps to reduce environmental

pollution and production costs. In this study, the benefits of dry machining were explored. Compressed air was used during dry cutting to clear of machined loose chips adhering to the hole surface, which helps to prevent the ignition of magnesium chips. Mineral oil-based cutting fluid (Almag®) was selected for the test due to its low viscosity and is a preferred choice for machining of magnesium alloys. The absence of water in this product prevents the formation of heat and explosive hydrogen while cutting magnesium foams. It has been shown that cryogenic machining is more suitable for producing favorable surface machining induced stresses during machining AZ31-O magnesium alloys [18]. In this study, liquid nitrogen-based cryogenic cooling (pressure- 3 bar) was applied through a delivery hose (Figure 3.2)

### 3.3. Machining Force, Surface Roughness, Burr Formation, and Chip Morphology

A KISTLER™ 9129AA three-channel dynamometer was used along with a multichannel charge amplifier type 5080 to measure the drilling forces (uncertainty ±20N). It is well known that the in-service functional performance of a machined syntactic foam product depends on its surface quality and integrity. A Zeiss Smart proof ™ confocal surface analyzer was employed to investigate the bore surface roughness (Ra) on different locations of the hole. Average values were noted for each test condition. The machining induced surface defects were characterized using a Tescan SEM for different cooling conditions. During machining magnesium-based foams, enhanced plastic deformation of the matrix causes material side flow that leads to the formation of burrs [12,13]. In this study, the effect of the cooling method and volume fraction of alumina reinforcements in the foam on the type of burr formed was investigated.

Table 3. 3 Test factors

| Experiment Conditions | | |
|---|---|---|
| Microsphere | (Volume Fraction %) | 5%, 10%, 15% |
| Cutting Speed | m/min | 40-120 |
| Feed/tooth | Mm/tooth | 0.075, 0.2, 0.4, 0.6, 0.8 |
| Cutting Insert | Kennametal™ | TiAlN PVD coated<br>K10 Uncoated Carbide |

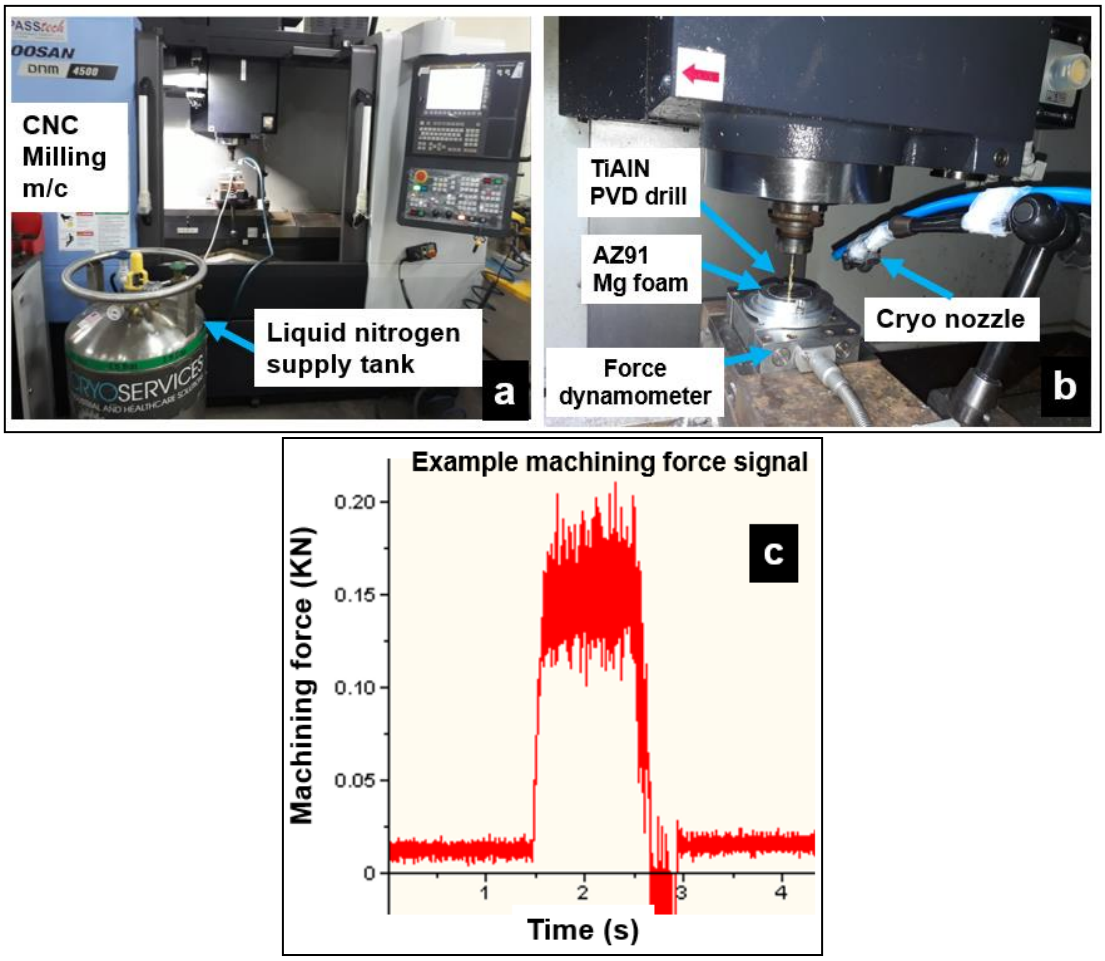


Figure 3. 2 a) Machine tool, b) drilling process and c) measured drilling force trace.

### 3.4 Finite Element Simulation

To understand the metal removal mechanism of magnesium syntactic foams, the material deformation in the cutting area was simulated by using AdvantEdge$^{TM}$, a finite element (FE) machining simulation program developed by Third Wave Systems USA.

AdvantEdge$^{TM}$ is a powerful tool for designing, setting up, improving, and optimizing machining processes. It enables users for determining machining parameters and tooling configurations that can reduce cutting forces, temperatures, and part distortion which are all done off-line. This reduces the need for experimental testing, which costs money and valuable production time. Direct benefits of AdvantEdge$^{TM}$ include:

• Reduces expensive cutting tests

• Prolongs tool life and reduces tool breakage

• Improves tool geometry and chip control

• Enable faster machining processes

• Have more efficient productivity

• Reduces part distortion due to heat generation, cutting forces, machining induced stress, etc.

• Increases material removal rates

• Increases machine utilization

AdvantEdge$^{TM}$ combines advanced finite element technology with a user-friendly graphic interface geared specifically for metal cutting simulations. 3D graphical user interface will be used. The cutting conditions and tool geometry used in the simulations were the same as those used in the experiments (Table 3.2 and Table 3.3). In this study, the Johnson-Cook constitutive material model is used to describe the effect of strain, strain rate and temperature on the flow stress of the AZ91-magnesium matrix and data as shown in Table 3.4 [5]. To simulate the drilling forces, the workpiece was developed as a homogenous isotropic material using 3 node triangle elements. The minimum and maximum element size for the cutting tool were 0.03mm and 0.3mm. For the workpiece, the minimum and maximum element size were 0.022 and 1.5mm. The workpiece thickness was 5mm. Friction model is based on Coulomb friction model. The friction coefficient employed in this study was in the range of 0.7.

**3.4.1 Material model**. The metallic material relationships between stress and strain can be described by the Johnson-Cook model under the conditions of large deformation, high strain rate and elevated temperatures. Being in a simple form and as it requires less effort to estimate the material constants, it has been widely employed by many researchers to predict the flow behavior of materials. The flow stress model is expressed as follows:

$$\sigma = (A + B\varepsilon^{n})(1 + C \ln\dot{\varepsilon}^{*})(1 - T^{*}m).$$

where $\sigma$ is the equivalent stress, and $\varepsilon$ is the equivalent plastic strain. The material constants are A, B, n, C, and m. A is the yield stress of the material under reference conditions, B is the strain hardening constant, n is the strain hardening coefficient, C is the strengthening coefficient of strain rate, and m is the thermal softening coefficient. The three parenthesis components in this equation represent, from left to right, the strain

hardening effect, the strain rate strengthening effect and the temperature effect, which influences the flow stress values. In the flow stress model, $\dot{\varepsilon}^*$ and $T^*$ are:

$$\dot{\varepsilon}^* = \frac{\dot{\varepsilon}}{\dot{\varepsilon}ref\dot{\varepsilon}}$$

$$T^* = \frac{T - Tref}{Tm - Tref}$$

where $\dot{\varepsilon}^*$is the dimensionless strain rate, $T^*$ is the homologous temperature, Tm is the melting temperature of the material, and T is the deformation temperature. $\dot{\varepsilon}ref$ and Tref are the reference strain rate and the reference deformation temperature, respectively [45].

Table 3. 4 Johnson cook Parameters [19]

| A | B | C | n | m | Strain Rate ref | $T_{ref}$ | $T_m$ |
|---|---|---|---|---|---|---|---|
| 140 | 605 | 0.03 | 0.52 | 0.32 | 1 | 20 | 533 |

In order to model the magnesium matrix behavior, the Johnson cook material model which is available through AdvantEdge$^{TM}$ software. To provide more flexibility with constitutive models. The yield surface determines when a material model will switch from elastic to plastic and calculates stress for a given strain; therefore, only experienced users should define these parameters. The user can define up to 100 state variables; however, only the first five will be displayed. This will allow users to describe more advanced UDYS constitutive models. These state variables can be updated at each time step, enabling implementation of damage models. The material model for this research is based on Johnson and Cook model.

**3.4.2 Friction model.** The friction coefficient between the tool and workpiece can have significant effects on simulation results. AdvantEdge$^{TM}$ uses a friction coefficient as defined by Coulomb friction. The Friction Coefficient window will appear, and the user can activate either the Default or User Defined radio button. Selecting the User Defined radio button allows the user to manually enter the friction coefficient. The friction coefficient is constrained by AdvantEdge$^{TM}$ to be between 0 and 1.

**3.4.3 Boundary conditions**. The regions of the workpiece where the tool is not in contact will be constraint in horizontal and vertical directions. Also, the right side

and the topmost side of the tool are constrained in the X, Y & Z directions. The maximum number of nodes used in the simulation is 24000.

**3.4.4 Simulation methods**. The thrust force results of the simulation analysis are validated through comparison with the experimental values. Moreover, the model gives a better understanding of how the foam behaves under machining, which includes the interactions between tool and particles, tool and the matrix, and particles and the matrix. The analysis also gives a clear explanation about closed foams and its effects. More importantly, the results help understanding which parameters (i.e., microsphere size and volume fraction of the microspheres) are affecting the thrust force. Lastly, comparison of the surface of the chip from the simulation with that obtained from the experiment was conducted.

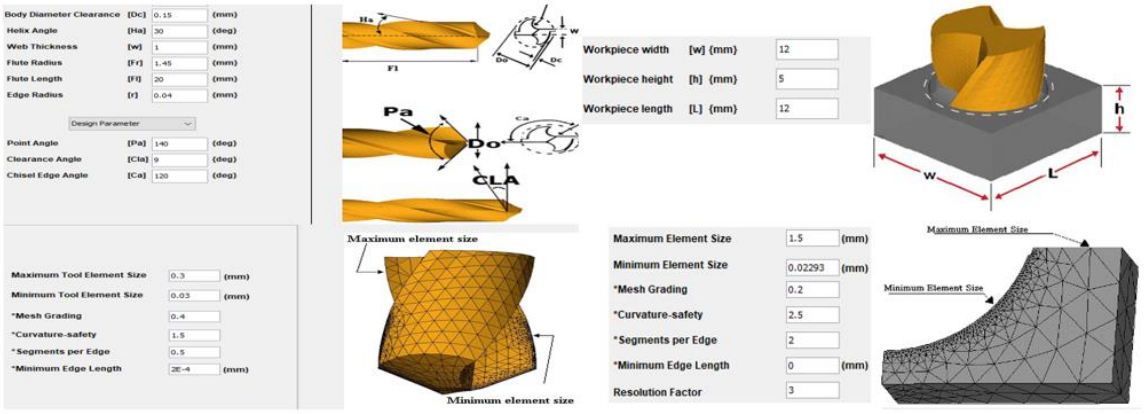


Figure 3. 3 Tool and workpiece mesh settings

### 3.5 Machining Induced Stress Measurements

The following figure shows the setup for machining induced stress measurements in radial, axial, and hoop directions accordingly. It is important to acknowledge the values for these stresses to avoid crack growth and propagation in the machined surface and to analysis the effect of drilling parameters and coolant type on the stress generation. The hoop stress was calculated along the circumference of the workpiece hole, the axial stress was measured through the hole depth as the tool go inside while the radial stress was calculated in the thickness of the hole towards the bulk of the material. All stresses were measured at 10 µm from the tool tip in the bore region where highest values of stress were generated.

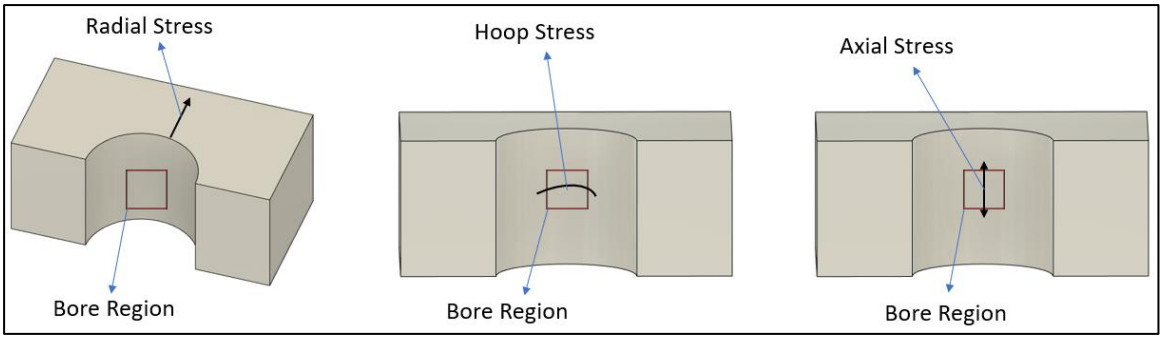


Figure 3.4 Machining induced stresses along radial, axial, and hoop directions, respectively.

### 3.6 Damage Mechanism

A unit cell model was developed to investigate the damage mechanics of ceramic microsphere, A custom workpiece with one hollow microsphere was designed for this study. The goal was to have a better understanding how the microsphere will collapse at different diameters and wall thicknesses. The next graph highlights the mesh settings for the unit cell model in AdvantEdge$^{TM}$. Figure 3.5 shows the orientation and positions of tool, magnesium matrix and hollow microsphere, respectively. The distance between the tool tip and the microsphere was set to be twice the diameter of the microsphere. In this model, three different diameters were investigated, and three wall thicknesses were also studied to highlight the damage model and the influence of these parameters on the thrust forces and the machining induced stresses.

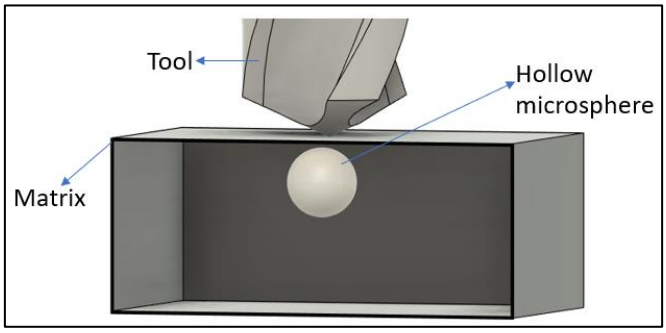


Figure 3.5 Unit cell model, tool, AZ91 matrix and Alumina hollow microsphere orientation

Finite element meshing parameters are shown in Figure 3.6. as for the minimum visible diameter in the software “2 mm”; the parameters for meshing were selected carefully. The maximum and minimum size of element were 0.5 and 0.02 mm, respectively. For

boundary conditions the top surface of the tool was selected as its boundary condition, while for the workpiece the bottom surface was selected.

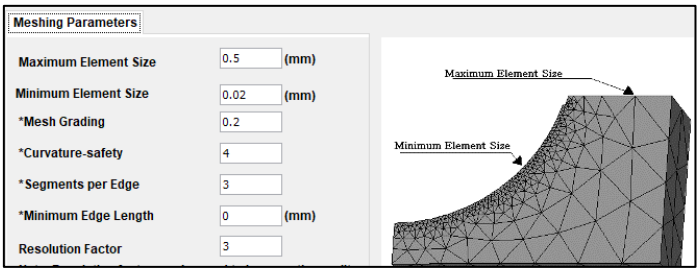


Figure 3. 6 Meshing parameters for Unit Cell model

# Chapter 4. Results and Discussion

## 4.1. Drilling Thrust Force

Figure 4.1 (a) shows the variation in thrust forces generated during drilling AZ91-magnesium syntactic foams reinforced with 15% alumina ceramic microspheres. The cutting test was carried out using TiAlN PVD coated twist drills under cryogenic cooling conditions. Thrust forces increased by 64% from 110N to 180N as the cutting speed decreased from 100 m/min to 25 m/min. Through mechanical testing, AZ91-magnesium foam is shown to undergo brittle fracture [13]. At higher cutting speed, a higher rate of shear loading acts on the material. This induces the thermal softening of the magnesium matrix and ceramic hollow microspheres to be fractured. A preferential propagation of brittle cracks along the shear zone could result. A reduction in shear plane length, chip-tool contact area, and friction force are expected at higher cutting speeds. This could be the possible reason for the reduction of thrust force. Figure 4.1 (b) shows the thrust force generated while cutting AZ91 magnesium foam at a range of feed/rev values and at 40m/min cutting speed. Machining using a TiAlN PVD coated drill under liquid nitrogen cooling conditions showed an increase in thrust force values by 175N when the feed was increased from 0.075 mm/rev to 0.6 mm/rev. This is an almost 233% increase in the magnitude of thrust forces, which was recorded as 75N and 250N at lower and higher feed values. This is primarily attributed to an increase in the chip-tool contact area and eventually chip load leading to higher values of thrust force. The role played by hollow ceramic microspheres in controlling the work hardening behavior of the magnesium matrix is primarily shown as the reason for higher force values. However, as the cutting feed is increased to 0.8 mm/rev, a drop in thrust force values is observed. A reduction of thrust force by 15% is noticed as the feed/rev value is increased from 0.6 mm/rev to 0.8 mm/rev. It is shown in the literature that the stress-strain behavior of AZ91 magnesium material is dependent on the temperature [35]. At temperatures lower than 150 °C, high material work hardening with high flow stress due to increased dislocation storage has been reported. With further increasing temperature, the stress-strain curve shows almost zero work hardening rate associated with reduced flow stress [35]. This interrelationship between work hardening and thermal softening could explain for the observed trend of cutting forces recorded during drilling AZ91 magnesium syntactic foams.

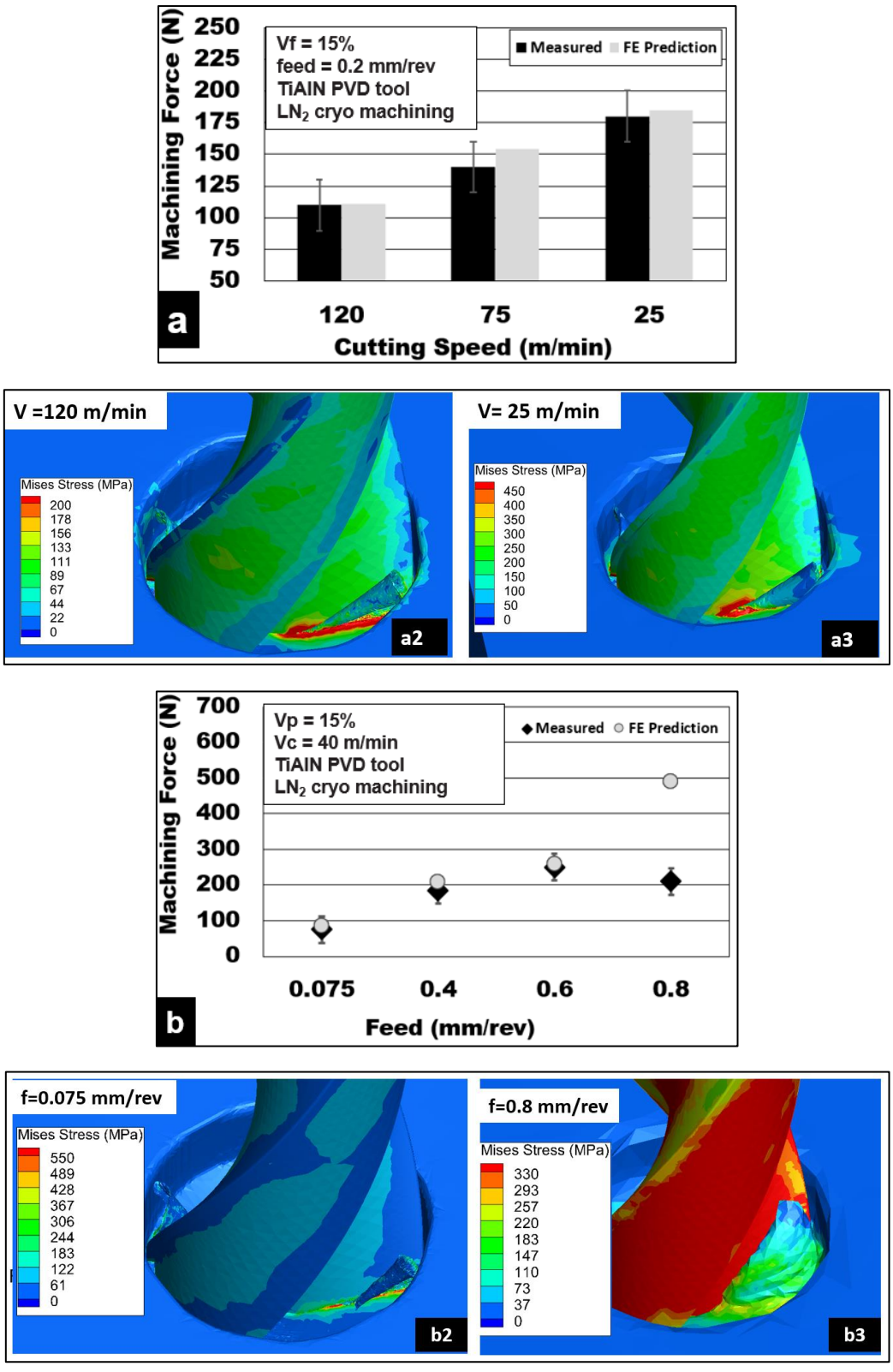


Figure 4. 1 Effect of process parameters during machining AZ91-15% magnesium foam; (a) effect of cutting speed, and (b) effect of feed in mm/rev.

The influence of volume fraction of hollow alumina microsphere reinforcements on the thrust forces generated during cutting AZ91 magnesium foam is shown in Figure 4.2. An increase in volume fraction increases the number of microspheres in the magnesium matrix. Along with the second phase precipitates of Al and Zn, the role played by the ceramic alumina reinforcements in enhancing the work hardening behavior of the magnesium matrix is significant [12]. The presence of these reinforcements affects the extent of plastic deformation of these foams through a characteristic load transfer that enables them to improve their peak strength. It is reported that the higher the number of ceramic hollow alumina in the magnesium matrix, the lower the plasticity of the foam [12]. A reduced ductility and strain to fracture are reported with a higher volume fraction of hollow microspheres, indicating an increase in its brittleness [12,13]. While cutting AZ91 magnesium foam under the cryogenic cooling method, an increase in thrust force by 50% while cutting with increasing volume fraction (15%) is observed. At a lower volume fraction of hollow alumina (5%) the drilling thrust forces were in the range of 135N, which increased to around 200N while cutting magnesium foam with 15% vol of alumina. This increase in thrust force is primarily attributed to the increase in peak compressive strength of the magnesium foam with the increasing volume fraction of ceramic alumina reinforcements. However, during dry machining, the increase in thrust forces recorded was almost 200% when the volume fraction of hollow alumina was increased from 5% to 15%. In general, it is observed that the thrust forces generated during dry machining were lower than the cryogenic machining for all volume fraction magnesium foams considered in this study. For 5% volume fraction AZ91 foams, the thrust forces generated during cryogenic machining were 170% higher than the dry machining. However, as the volume fraction of hollow alumina increased to 15%, the force margin reduced to 35%. This phenomenon indicates the increasing brittleness of the magnesium foam with increasing ceramic alumina microspheres and their effect on the plastic deformation of the AZ91 magnesium matrix.

It is observed from the experiment results that the method of cooling/lubrication plays an important role in the generation of thrust forces during drilling AZ91-magnesium foams. Figure 5a shows the measured thrust forces during cutting AZ91-15% hollow alumina syntactic foams under three different cooling methods as shown in Figure 4.2 (a). As expected, cryogenic machining using liquid nitrogen generated the highest thrust forces (200N), which were 33% higher than the dry machining (150N). In general, of all cutting conditions, wet machining using the Almag® mineral oil generated the

lowest thrust force (120N), which was 40% and 20% lower than cryogenic machining (200N) and dry machining (150N), respectively.

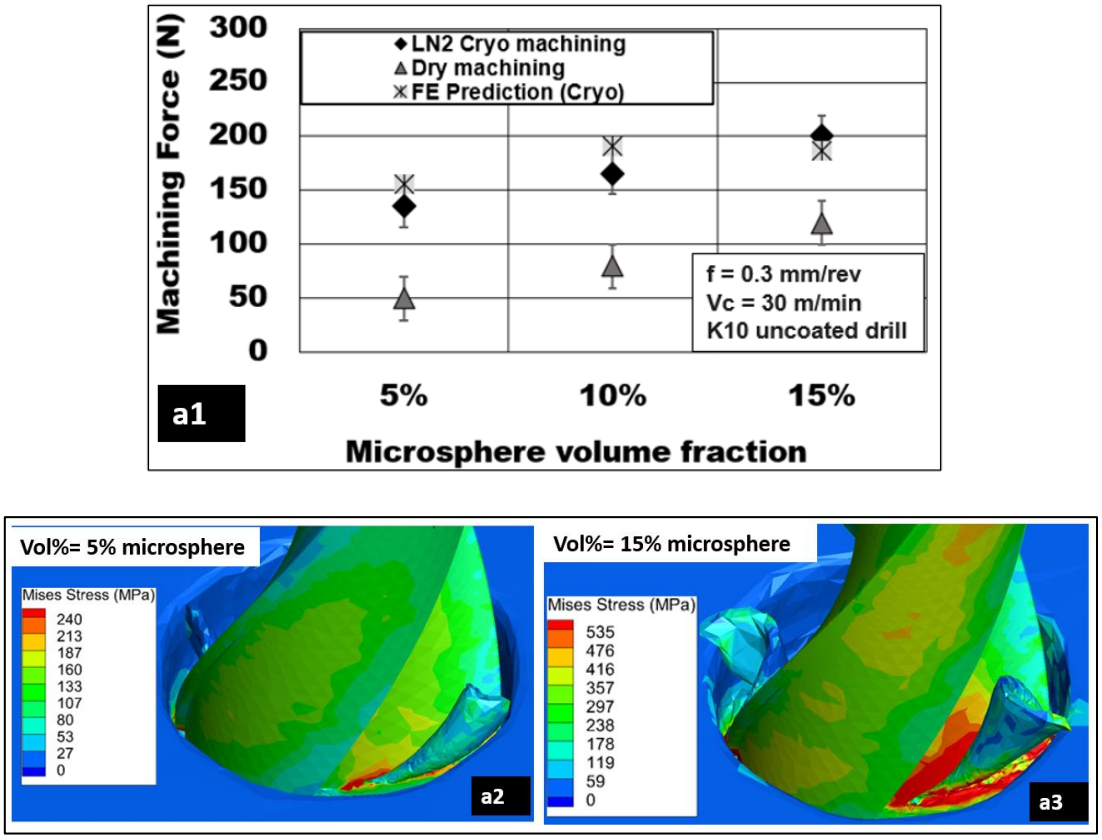


Figure 4. 2 Effect of alumina volume fraction on thrust force during machining AZ91-magnesium foam.

The application of liquid nitrogen increases the hardening behavior of the AZ91 magnesium matrix. The brittle material behavior is promoted due to subzero temperatures in the cutting zone. Through mechanical testing under cryogenic conditions, it is shown that the yield compressive strength and peak compressive strength are increased while the ductility and strain to fracture of the magnesium foam are reduced [12,13]. This transition in deformation behavior to brittle type and a resultant increase in material hardness could be the possible reason for the higher magnitude of recorded thrust forces under cryogenic machining conditions and agrees well with the reported literature [39]. Under cryogenic cutting conditions, initiation and propagation of reinforcement/matrix interface longitudinal crack and transverse matrix cracks favor the formation of discontinuous chips. A transformation in the plastic deformation behavior of the material is indicated through measured thrust forces with variation in cooling methods. The thrust forces measured during dry machining conditions were 25% higher than cutting using Almag® Oil. The presence of mineral

oil in the cutting zone helps to minimize adhesion of the magnesium matrix and reduce the generation of thrust force. The lubrication effect is maximized with the application of Almag® Oil, which helps to reduce BUE and friction [40]. Thus, it is a more preferred coolant for light machining of magnesium alloys. Whereas during dry machining, the heat generated during the shearing process is dissipated into the cutting zone leading to the thermal softening of the magnesium matrix. This phenomenon promotes adhesion of soft magnesium with increasing BUE formation and friction. Under these conditions, a highly plastic magnesium matrix is encouraged to yield much earlier than the alumina microsphere. This causes the load to be transferred through the interface leading to longitudinal cracks and reinforcement debonding [13]. This phenomenon explains the effect of the cooling/lubrication method on the magnitude of thrust force generated during machining AZ91 magnesium reinforced with 15% hollow alumina metallic foam.

Figure.4.3 (b) shows the effect of tool coating on experiment thrust force. As seen from the results, during cryogenic cooling conditions, drills with TiAlN PVD coated tools generated 25% lower thrust forces than the uncoated K10 carbide drills. As discussed earlier, the use of liquid nitrogen tends to increase the hardness and peak compressive strength of the metallic magnesium foam. Subzero cooling conditions enhance the brittle behavior of the magnesium foam. Cutting tool wear is shown to accelerate under cryogenic conditions [21]. The contribution to tool abrasion arises due to the rubbing of hollow ceramic microspheres in tandem with hardened magnesium matrix. The presence of the tool coating reduces the tool abrasion and helps to extend the tool life. The cutting edge is expected to wear rapidly due to high friction, the formation of BUE, and due to diffusion at higher temperatures. However, TiAlN PVD coated tool possesses a good nano hardness of 35 GPa, reduced coefficient of friction, and high-temperature operation (700$^{\circ}$C) [41]. This helps in the reduction of generated thrust forces while cutting with TiAlN PVD coated cutting tools.

Table 4.1 shows the different parameters used in experimental and simulation. The first column indicates machining parameters such as cuttings speed and feed rates. It includes the volume fraction of the hollow microspheres, tool coating, coolant method, and different inserts. Total number of samples were fourteen as shown in Table 4.1. three samples for different cutting speeds, four for different feed rates and three for different hollow microsphere volume fraction. Seven experiment and simulations conducted for Tool 1 and seven tests for tool 2. The last column indicates the error percentage between the experimental data and simulation data.

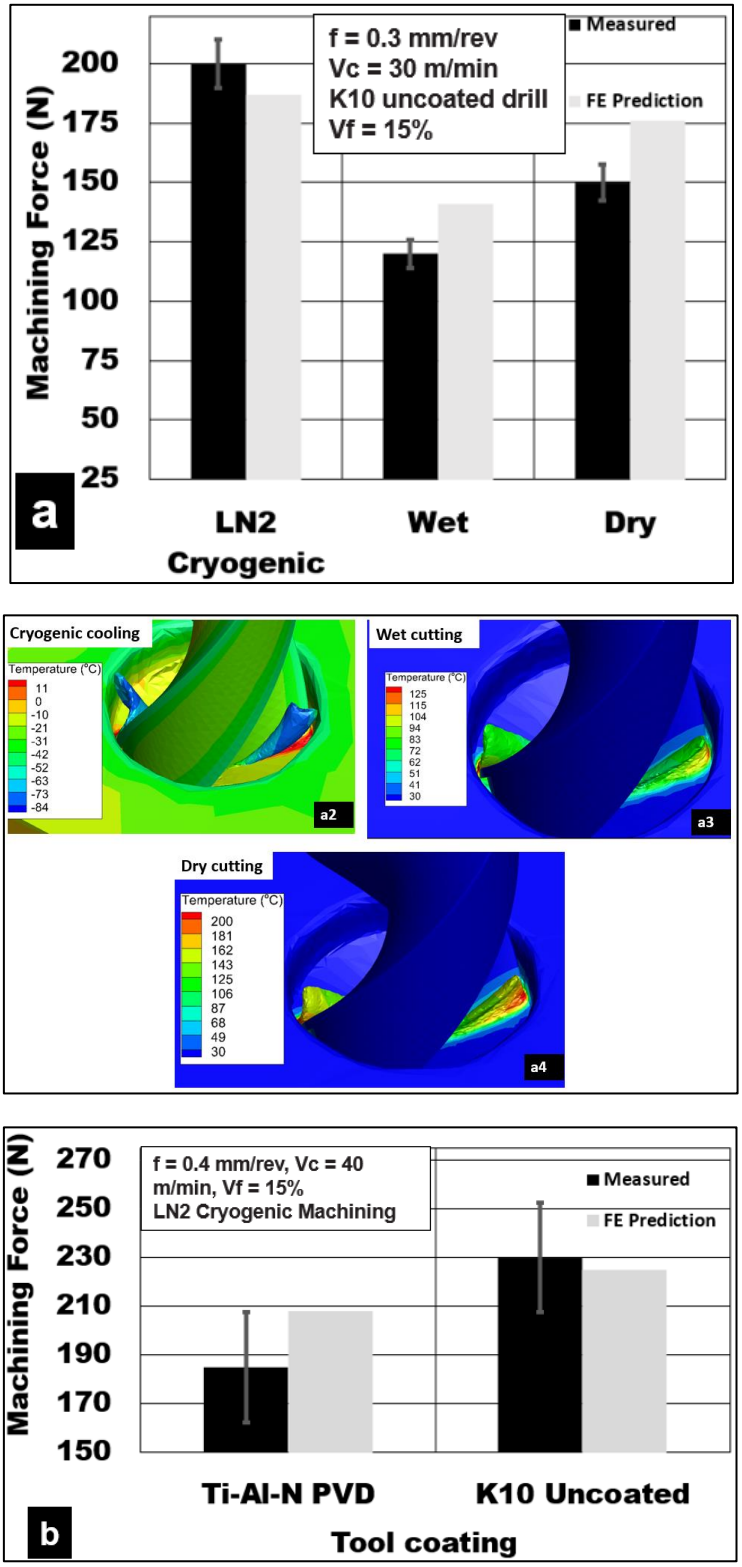


Figure 4. 3 Effect of a) type of coolant and b) tool coating on thrust force during machining of AZ91-15% magnesium foam.

Table 4. 1 AZ91 with hollow alumina drilling parameters

| | AZ91-Alumina-Cryogenic Drilling | | | | | | | | | |
|---|---|---|---|---|---|---|---|---|---|---|
| | Bubble size mm | Volume Fraction | Tool | RPM | Cutting Speed (m/min) | Feed per rev (mm/rev) | Feed Rate mm/min | Measured Thrust Force N | Predicted FE Force | Error % |
| Cryo-Cutting speed | 0.3 | 15 | Tool 1 | 7643 | 120 | 0.2 | 1528.6 | 110 | 111 | 1% |
| | 0.3 | 15 | Tool 1 | 4777 | 75 | 0.2 | 955.4 | 140 | 154 | 9% |
| | 0.3 | 15 | Tool 1 | 1592 | 25 | 0.2 | 318.4 | 180 | 185 | 3% |
| Cryo-Feed rate | 0.3 | 15 | Tool 1 | 2547 | 40 | 0.075 | 191 | 75 | 85 | 12% |
| | 0.3 | 15 | Tool 1 | 2547 | 40 | 0.4 | 1018 | 185 | 208 | 11% |
| | 0.3 | 15 | Tool 1 | 2547 | 40 | 0.6 | 1528 | 250 | 259 | 3% |
| | 0.3 | 15 | Tool 1 | 2547 | 40 | 0.8 | 2037 | 210 | 490 | 57% |
| Cryo-Vol% | 0.3 | 5 | Tool 2 | 1910 | 30 | 0.3 | 573 | 135 | 156 | 13% |
| | 0.3 | 10 | Tool 2 | 1910 | 30 | 0.3 | 573 | 165 | 191 | 14% |
| | 0.3 | 15 | Tool 2 | 1910 | 30 | 0.3 | 573 | 200 | 187 | -7% |
| Cryo-Tool Coating | 0.3 | 15 | Tool 2 | 2547 | 40 | 0.4 | 1018 | 230 | 225 | -2% |
| Cryogenic | 0.3 | 15 | Tool 2 | 1910 | 30 | 0.3 | 573 | 200 | 187 | -7% |
| Coolant | 0.3 | 15 | Tool 2 | 1910 | 30 | 0.3 | 573 | 120 | 141 | 15% |
| Dry | 0.3 | 15 | Tool 2 | 1910 | 30 | 0.3 | 573 | 150 | 176 | 15% |

### 4.2 Surface Quality and Integrity

Figures 4.4 (a) and 4.4 (b) show the effect of process parameters on achievable surface quality during cutting AZ91-magnesium metallic foam. As can be seen from the graphs, an increase in cutting speed from 25 m/min to 100 m/min results in an increase in average surface roughness Ra values by 52%. Best surface quality with a Ra value of 0.48 µm was achieved at lower cutting speed under cryogenic cooling conditions. On the other hand, the average surface roughness (Ra) increased by 364% as the feed value increases from 0.075 mm/rev (0.39 µm) to 0.8 mm/rev (1.81 µm) during cryogenic cutting using TiAlN coated drill. Larger the feed, the higher the volume of metal removed, wider and deeper the feed marks, resulting in higher average surface roughness values.

The influence of different cooling methods on achievable surface quality during drilling AZ91-magnesium metallic foam using uncoated K10 drill is shown in Figure 4.5a. The experiment results show that surface roughness values during cryogenic machining (0.73 µm) reduced by approximately 55% and 43% compared to wet machining (1.6 µm) and dry machining (1.3 µm), respectively.

Thrust forces recorded during cryogenic machining were generally higher by 30% to 40% compared to dry and wet machining. This is primarily due to the hardening behavior of the magnesium foam due to a drop in cutting temperature.

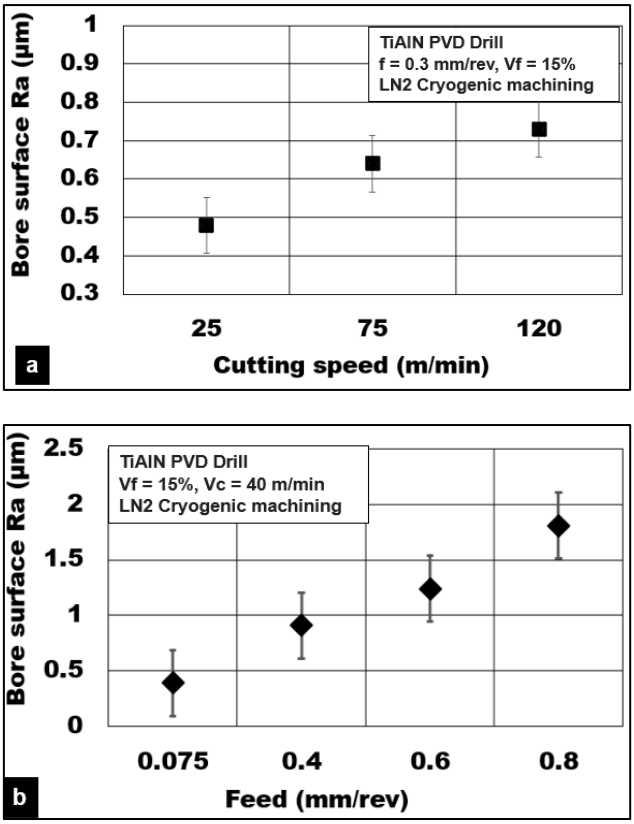


Figure 4. 4 Effect of process parameters a) cutting speed and b) feed on machined bore surface roughness (Ra) during machining of AZ91-15% syntactic foam.

SEM investigation of the bore surface shows smaller feed marks, less machining induced surface defects, and lower matrix plasticity in the form of material side flow (Figure 4.5 b). Under these cooling conditions, the brittle nature of the material helps to produce smaller discontinuous chips resulting in good surface quality (Ra between 0.3 to 0.5 µm). During wet machining using mineral oil, the effects of 2-body tool abrasion and adhesion of the magnesium matrix to the cutting tool are reduced to a certain extent. However, the SEM investigation of the drilled bore surface shows certain areas comprising of bore pits and voids. This is primarily attributed to flushing away of the loose, brittle particles that form on the top layer of the machined surface by the viscous mineral oil, which was applied under pressure (Figure 4.5 c). During dry machining, the plastic deformation of the magnesium matrix is found to be the key deformation mechanism that affects the surface quality. The average surface roughness values measured on holes drilled under dry machining were 20% lesser than wet machining conditions. Hole samples investigated using SEM showed slightly wider and deeper feed marks primarily due to material side flow. Rewelding of finer chips and smearing of the machined surface were some of the surface defects observed. An

increase in shear zone temperature during dry cutting causes adhesion of finer pieces of chips resulting in deterioration of surface quality (Figure 4.5d).

Figure.4.6 shows some of the commonly observed machining induced defects during drilling AZ91-magnesium reinforced with hollow alumina microspheres under different cooling conditions. Overall, the surfaces produced by cryogenic machining were of good quality. However, few of the edges along the hole exit side were subjected to delamination due to the disintegration of the burr roots (Figure 4.6a). This indicates the brittle nature of the material machined due to exposure to subzero cutting temperatures. On the other hand, wet machining using a viscous mineral oil produced surfaces that comprised of flushed away particles leading to unexpected pits at certain locations on the bore section of the drilled hole (Figure 4.6c, 4.6d). This shows the significance of the application of mineral oil under pressure, which could affect the attainable surface quality and integrity by washing away the disintegrated particles on the drilled surfaces leading to empty spaces in the matrix. In addition to this, some locations on the hole exit side had delaminated edges and thin material push off. During dry machining, the shear zone temperature allows the plastic flow of the magnesium matrix around the ceramic microsphere, initiating interface debonding and preferential cracking (Figure 4.6d). Voids created by microsphere pull out from the matrix is closed at a faster rate due to accelerated densification of the magnesium matrix. [13]. The extent of plastic deformation undergone by the magnesium matrix is greater under dry machining compared to wet and cryogenic machining. This damage mechanism is visible in the form of smearing of side flow material along the tool feed tracks (Figure 4.6 b).

Figure. 4.7 a show the effect of volume fraction of hollow alumina microspheres on the achievable surface quality during drilling AZ91-magnesium foams. Under cryogenic machining conditions using uncoated K10 drill, the average surface roughness value (Ra) increases by almost 92% as the volume fraction increases from Vf = 5% (0.38 µm) to Vf = 15% (0.73 µm) similar as observed in [29] . On the other hand, during dry machining with the same tool, the average surface roughness value (Ra) increases by 72% as the volume fraction increases from Vf = 5% (0.76 µm) to Vf = 15% (1.3 µm).

The percentage of ceramic microspheres present in the magnesium matrix greatly affects the plastic deformation characteristics of the AZ91 foam. In this work, within the range of foam volume fractions tested, it is seen that an increase in the number of hollow ceramic microspheres in the matrix results in a foam that behaves like a brittle foam.

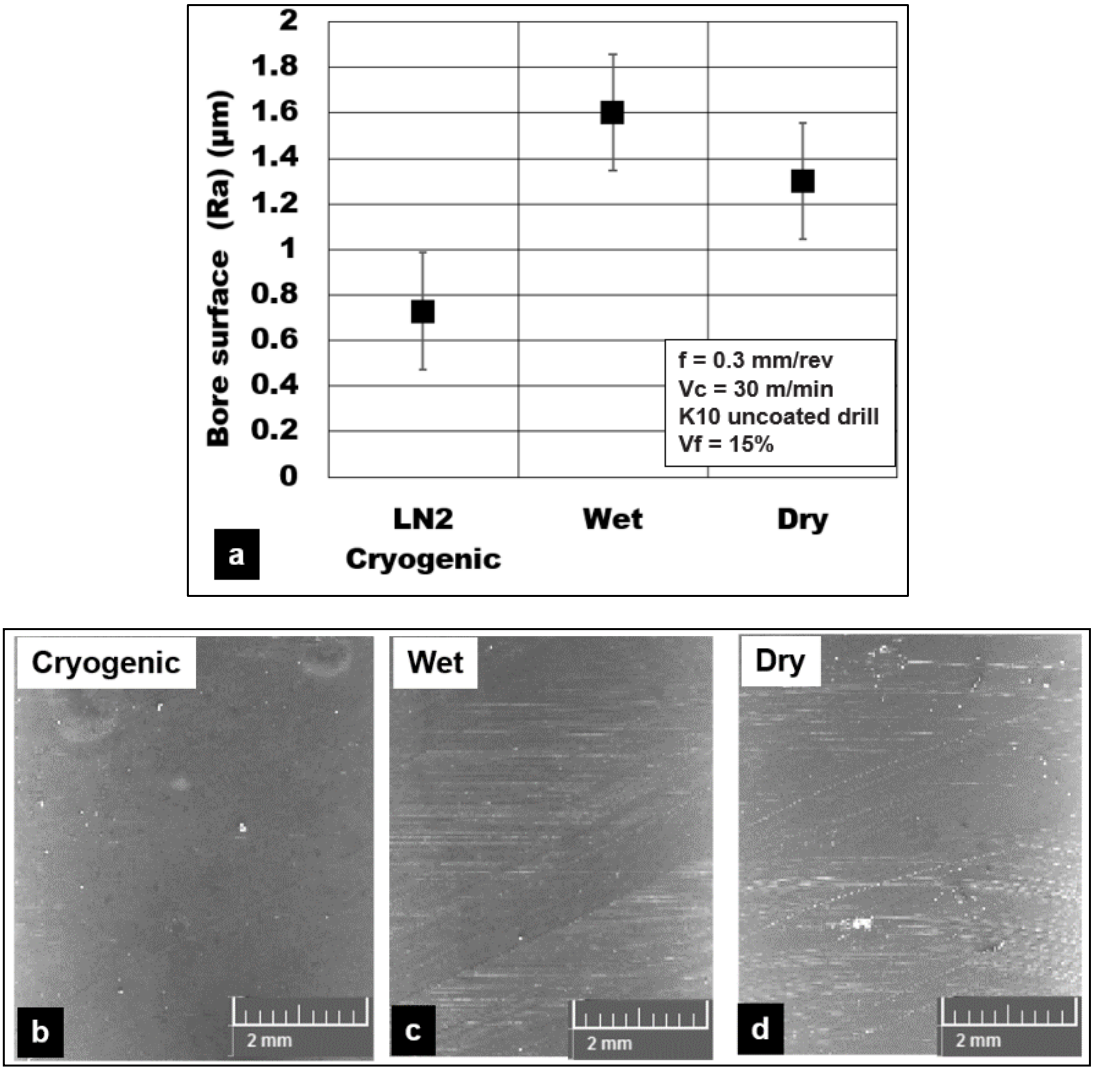


Figure 4. 5 Effect of coolant on machined bore surface roughness (Ra) during machining of AZ91-15% alumina syntactic foam.

The number of defect initiation points increases with volume fraction. Hence the average surface roughness measured under both cryogenic and dry machining conditions correlates well with the SEM observation. Figure. 4.7b shows the bore surface roughness values (Ra) during cryogenic cutting of AZ91 magnesium-15% alumina foam. It is observed that the TiAlN PVD coated tool (Ra: 0.91 µm) produces a surface with roughness values, which are 40% lower than the uncoated tool (Ra: 1.5 µm). This result shows the significance of tool coating in reducing friction due to the abrasion of ceramic microspheres and adhesion of magnesium chips. The selected TiAlN PVD coating is effectively shown to minimize the BUE and produce a comparatively good surface quality and integrity.

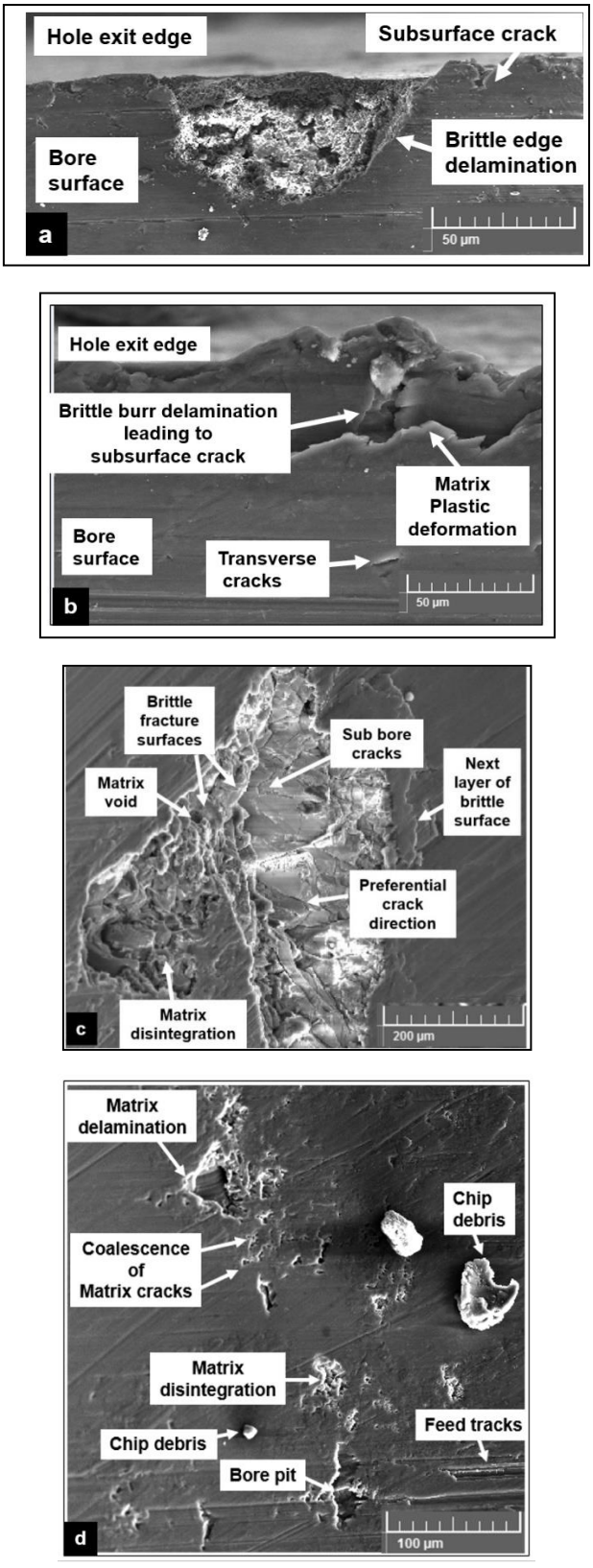


Figure 4. 6 Some of the commonly found drilling induced defects during machining of AZ91 magnesium-alumina syntactic foam (a. Cryogenic b. Dry, c, d. Wet cooling).

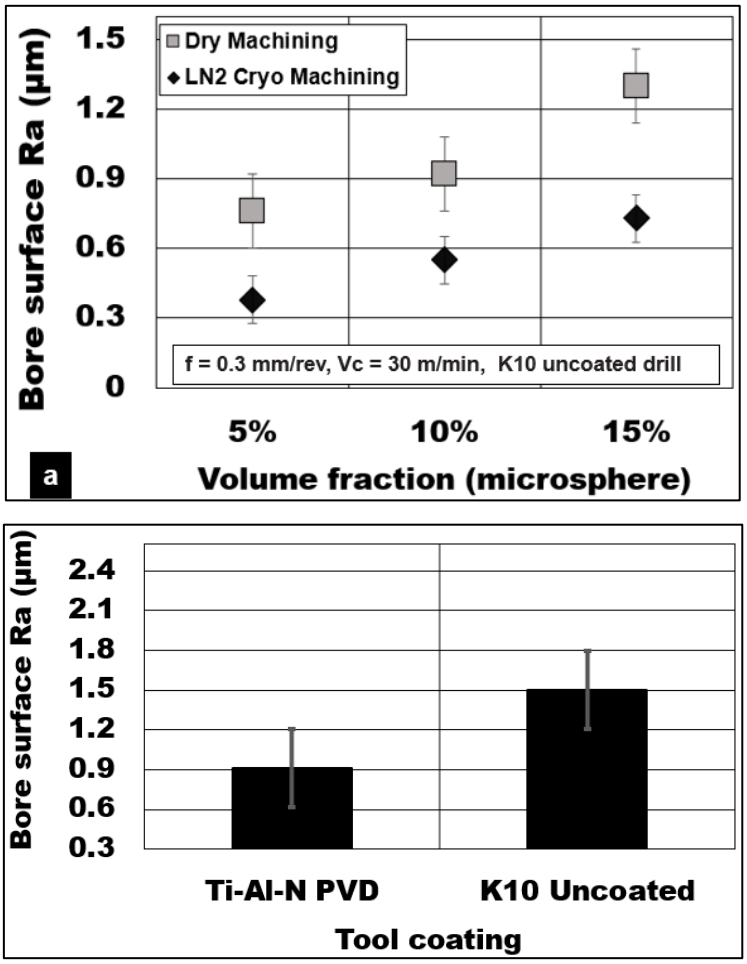


Figure 4. 7 a) Effect of hollow alumina volume fraction on bore surface roughness (Ra) during machining AZ91-magnesium foam b) effect of tool coating on Ra.

### 4.3 Machining Induced Stress

Machining induced stress is the stress generated in the workpiece material during the machining process and stayed inside the material after the load is released. For medical applications, this phenomenon is very dangerous, because the implant is inside

the body and any crack propagation resulted from internal machining induced stress might cause crack for the piece.

For this study as shown in the following figures, machining induced stresses were measured to investigate the influence of process parameters on the generation of this stress and to have a better vision of how the stress value will be after the force has been released, either negative “compression” or positive value which is “tensile”.

### 4.3.1 Effect of cutting speed.

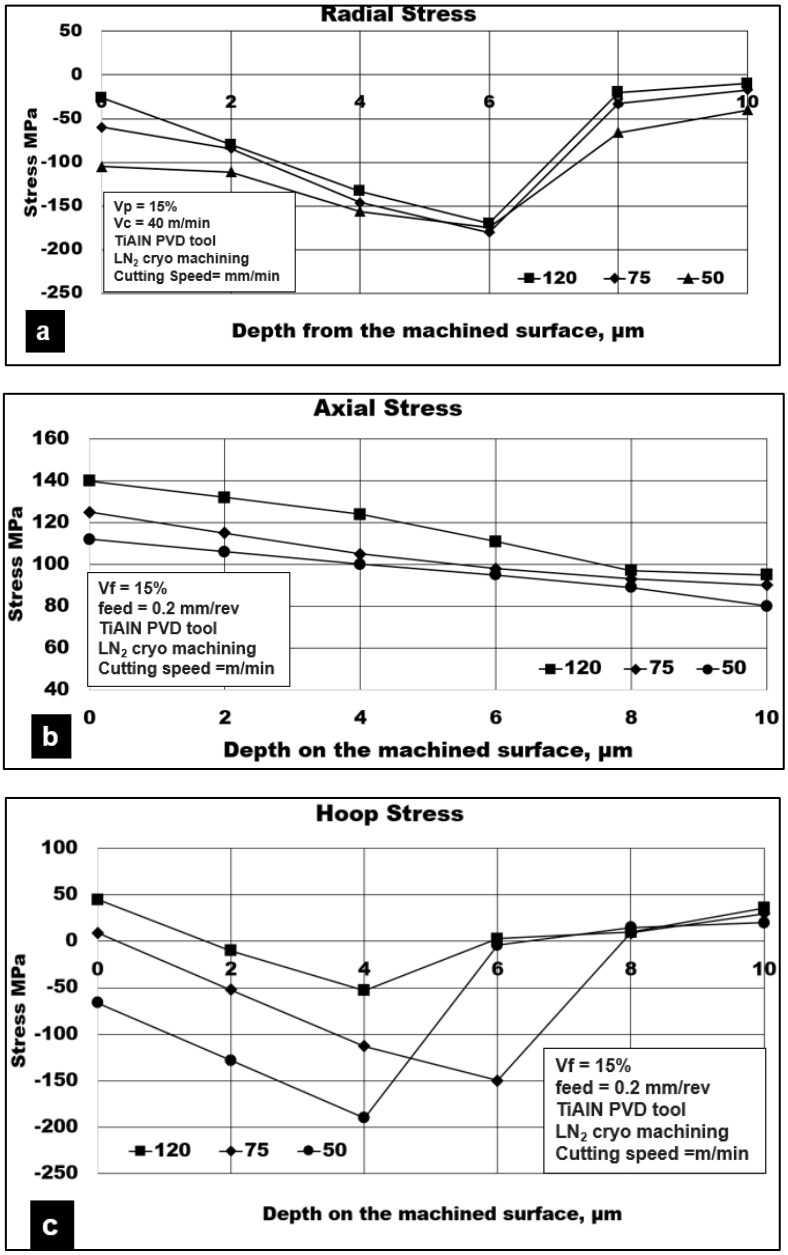


Figure 4. 8 Effect of cutting speed on the machining induced stress.

Figure 4.8 shows the effect of cutting speed on the machining induced stress during drilling AZ91-magnesium foams. Under cryogenic machining conditions using TiAlN PVD coated tool. The results show a tensile behavior when the speed is high and oppositely a compression one in the lower speed, this is due to heat generation in high speeds as compared to low cutting speed. The stress distribution along the radial direction is shown in Figure 4.8 a, while hoop and axial directions are shown in Figure 4.8 b and c, respectively. The graph trend shows a tensile stress in the first 3 microns from the tool tip followed by a compression stress until the force is released from the workpiece. A higher value of stress of 20 MPa tensile value in the machined surface at 120 m/min cutting speed compared to 60 MPa and 105 MPa compression value in case of 75 and 50 m/min cutting speed, respectively as shown in Figure 4.8 a.

### 4.3.2 Effect of feed rate.

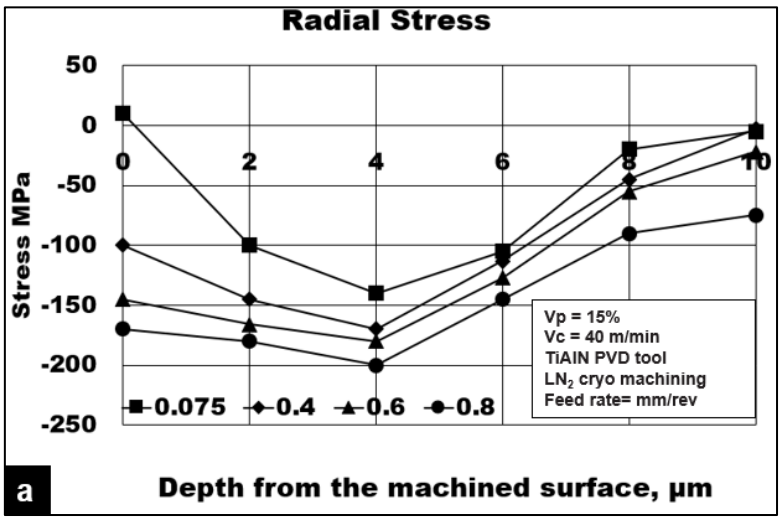


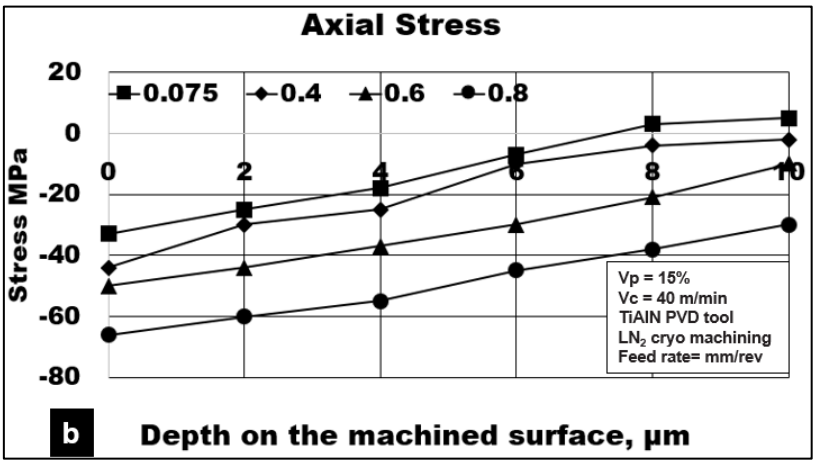

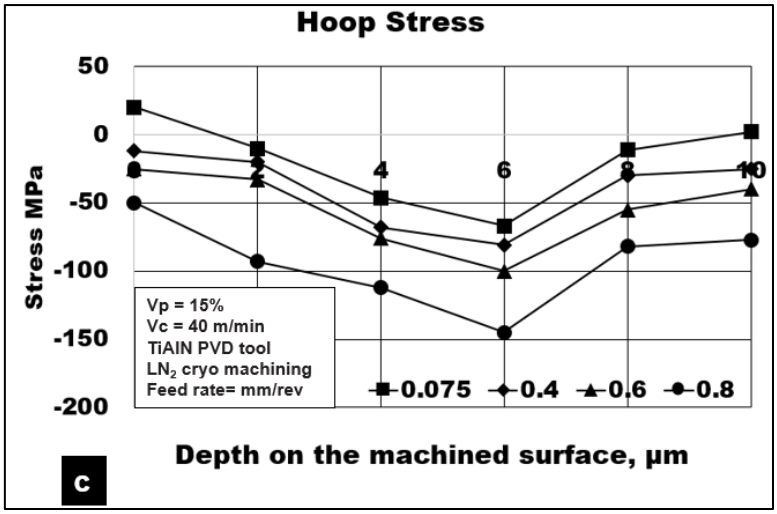


Figure 4. 9 Effect of feed rate on the machining induced stress.

Figure. 4.9 shows the effect of feed rate on the machining induced stress during drilling AZ91-magnesium foams. Under cryogenic machining conditions using TiAlN PVD coated tool. At low feed rate the machining induced stress tends to behave tensile and the opposite at high feed rate where the stress values are negative which are compression values. Drilling metallic syntactic foams at lower feed rates will cause rubbing to the surface and heat generation, this is the main reason of tensile induced stresses at 0.075 mm/rev feed rate. As shown in Figure 4.9 the value of stress is 10 MPa "positive" in case of low feed and 100, 145 and 170 MPa "negative" for the lower feeds in order from 0.4,0.6 and 0.8. A maximum tensile stress of 20 MPa in hoop direction was measured at 0.075 mm/rev feed rate, while compression stress of 50 MPa at 0.8 mm/rev feed rate was calculated in the circumference direction of the drilled hole as indicated in Figure 4.9 c.

### 4.3.3 Effect of microsphere volume fraction.

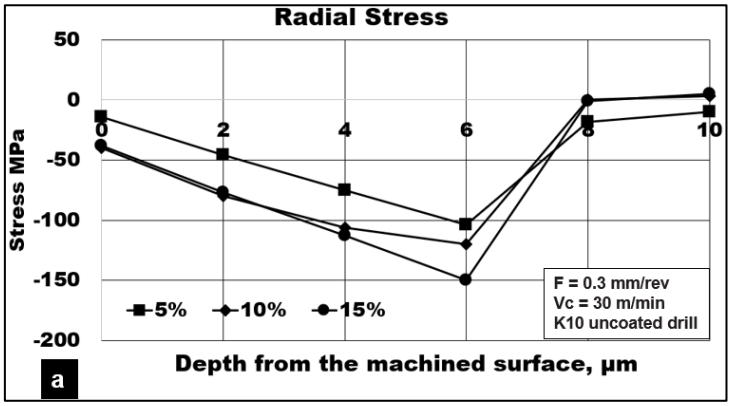

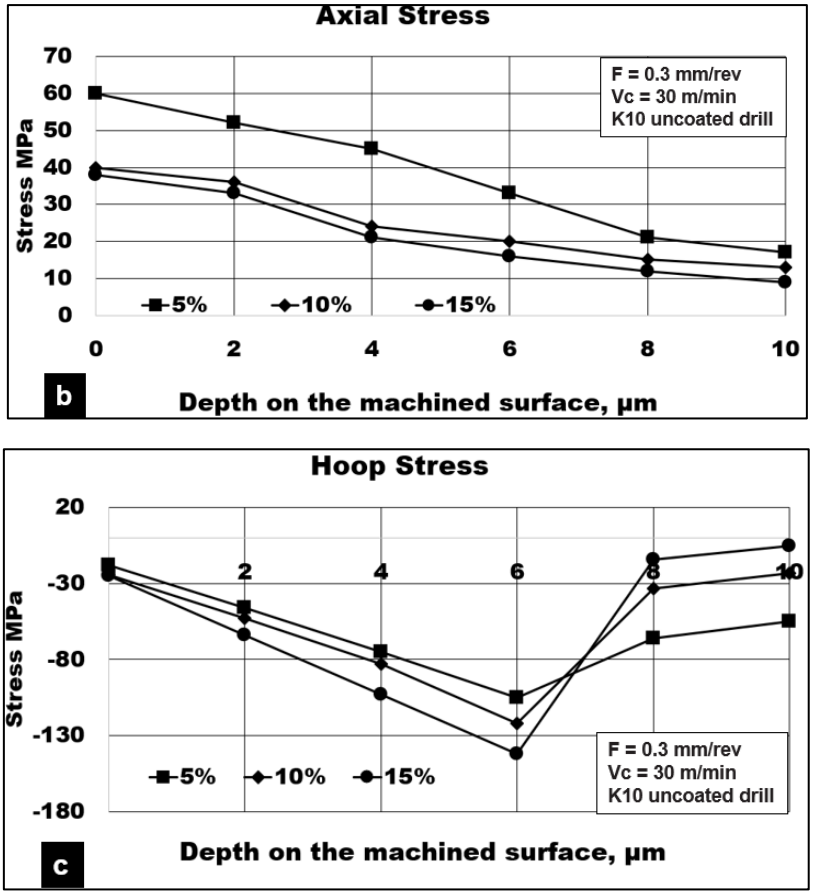


Figure 4. 10 Effect of Volume fraction on the machining induced stress

Hollow microsphere volume fraction from the total volume of matrix workpiece is one of the major parameters in this study. In Figure 4.10 the stress distribution in the machined surface was measured and how it was affected by the percentage of hollow microsphere volume fraction. As shown in the figure higher tensile stress generated at lower volume fraction in the radial, axial, and hoop directions, respectively. This due to the increase in microspheres number at lower percentage. Fig 4.10 b shows the stress distribution in the axial direction, a value of 60 MPa was measured for 5% volume fraction, on the other hand, values of 40 MPa and 38 MPa in case of 10% and 15% respectively. There is 2.8% decrease in radial stress values for 10% and 15% volume fraction compared to 5% volume fraction.

### 4.3.4 Effect of tool coating

Tool coting is a significant parameter in machining of syntactic foams. Figure 4.11 shows the effect of tool coating on the machining induced stress during drilling AZ91-magnesium foams

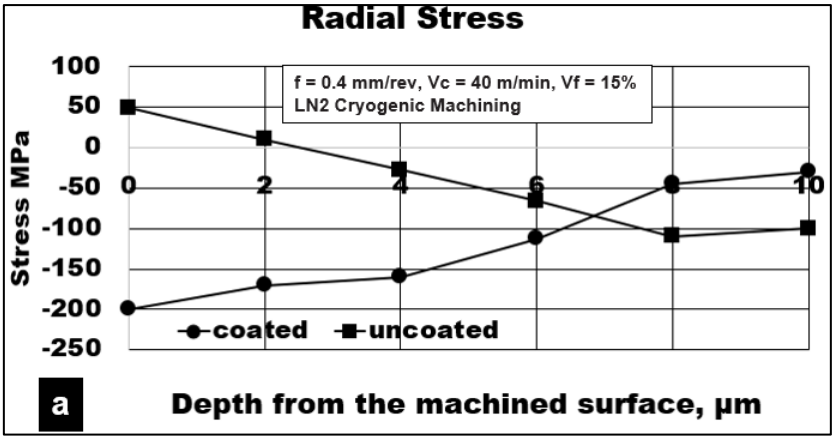


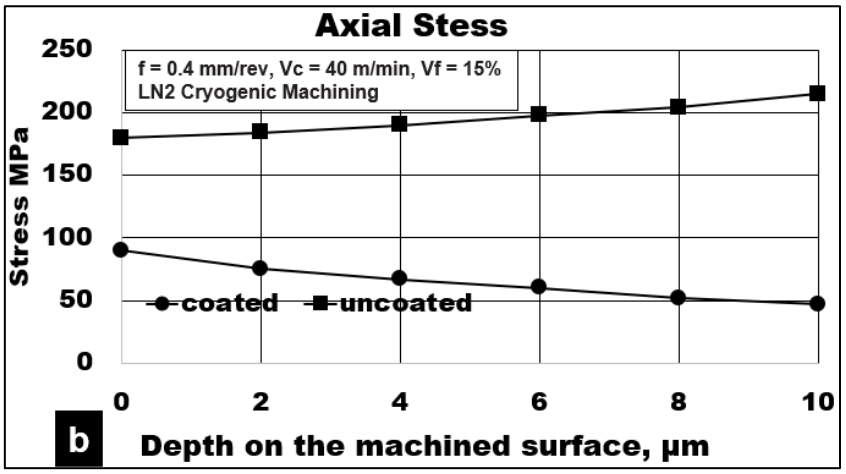


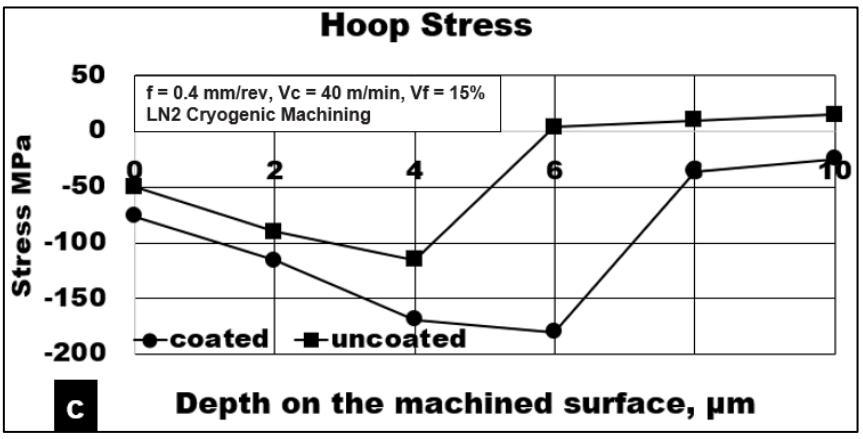


Figure 4. 11 Effect of tool coating on the machining induced stress

Under cryogenic machining conditions at fixed cutting speed and feed rate. It is indicated from the figure that there is clear compression behavior in drilling AZ91 magnesium foams using the coated tool. Fig 4.11 a shows the radial stress values, for the uncoated tool the value was 49 MPa in tensile sign. While for carbide coated tool, the value is more compression 328 MPa. For the axial stress, the uncoated tool recorded stress value was twice the value of TiAlN coated tool.

### 4.3.5 Effect of coolant type

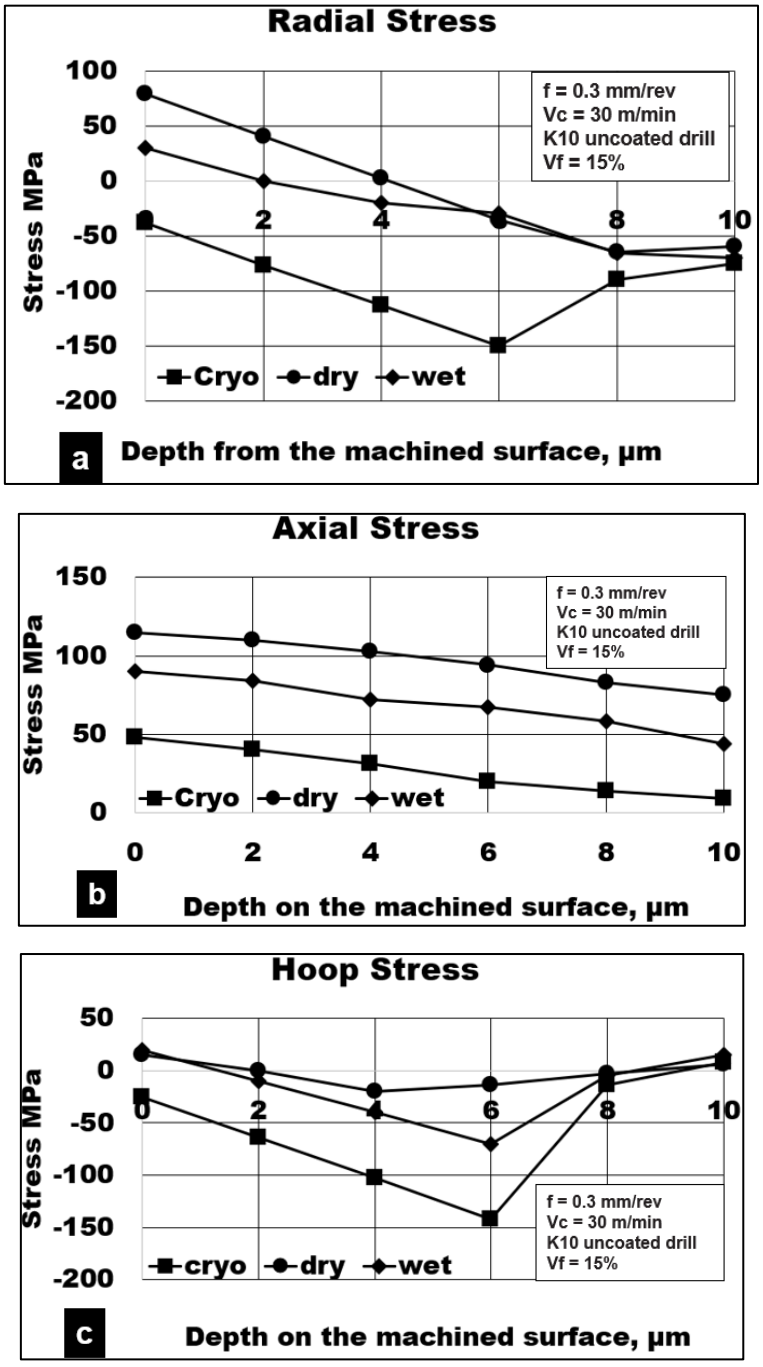


Figure 4. 12 Effect of lubrication method on the machining induced stress

Lubrication method effect on the machining forces and machining induced stresses is one of the key objectives of this thesis. The machining induced stresses were measured for cryogenic, wet, and dry conditions. At sub-zero degrees in case of cryogenic machining, the values of the machining induced stress tend to be more

negative “compression” compared to lubricant and dry conditions. Figure 4.12 shows the trend of the machining induced stress for different cooling techniques. Cryogenic cooling recorded compression value of 38 MPa in radial stress graph (Figure 4.12 a) while the wet machining value was 30 MPa tensile stress. The dry machining scored the highest value, which is almost the double in case of cryogenic, of 79 MPa tensile stress. For the axial stress as shown in Figure 4.12 b the recorded values were 48,90,115 MPa tensile stress for cryogenic, wet, and dry drilling, respectively as observed in [50].

### 4.4 Drilling Burr Formation

Burrs during plunge drilling are primarily formed due to thermo-mechanical loads that act on the material resulting in their push out as the tool exits the hole. Figure 4.13 shows the effect of the cooling method on the burr formation while cutting AZ91-magnesium reinforced with 15% hollow alumina syntactic foams. Burr height was measured at the entry and exit side of the hole using a Zeiss$^{TM}$ Smart proof confocal microscope, and the average value was recorded. It is observed that the burr height at the entry and exit side during cryogenic machining was 20 µm and 70 µm, respectively. These values are approximately 60% (entry) and 30% (exit) lower than the burr heights formed during dry machining. On the other hand, wet machining produced burrs, which were almost 95% (entry) and 22% (exit) higher than cryogenic machining and 13%-20% reduction compared to dry machining. In general, dry machining conditions produced higher values of burr height both at the entry (49 µm) and exit sides (96 µm) of the hole. During dry drilling, the heat generated in the cutting zone promotes the plastic deformation of the magnesium matrix that initiates material side flow. This is more pronounced during dry machining compared to wet and cryogenic machining conditions.

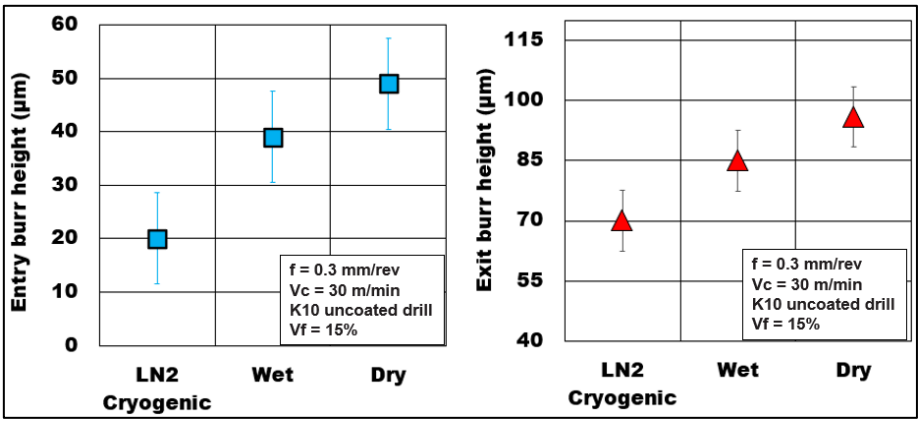


Figure 4. 13 Effect of coolant on burr height during machining AZ91-magnesium syntactic foam.

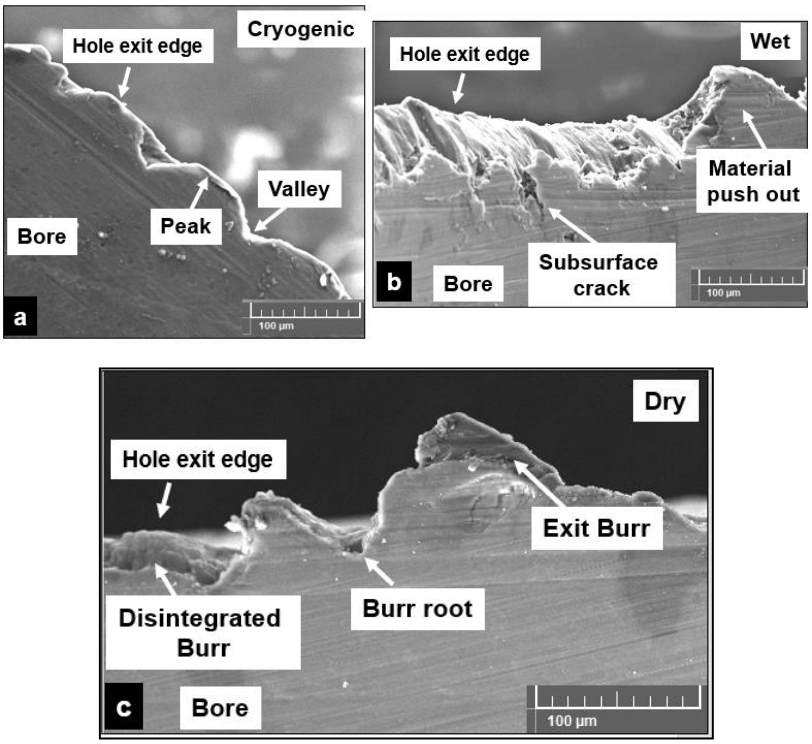


Figure 4. 14 Different types of edges produced at the hole exit side of the AZ91-15%magnesium foam a) Cryogenic b) Wet c) Dry. (Vc = 30m/min, feed = 0.3mm/rev, uncoated tool).

Investigations were carried out on the drilled burr forms produced using a VEGA 3 Tescan SEM (Fig. 4.14). It is noted that cryogenic machining using liquid nitrogen produces edges that are approximately sinusoidal in form. Due to a sudden drop in cutting temperature, the magnesium foam hardness is increased. This change in temperature conditions makes the magnesium matrix material behave more brittle than ductile. These conditions produce powdery chips that are caused due to the brittleness of the material. It is favorable to produce discontinuous chips, however, due to increased brittleness causes areas of hole edges to disintegrate. These machining induced defects caused due to cryogenic machining also develops as a subsurface crack as it propagates underneath the drilled surface. Small areas of magnesium matrix that still show some signs of plastic deformation form small scale burrs in some areas of the hole edge. However, most of the magnesium matrix being exposed to subzero temperature conditions, brittle behavior, is more dominant. This material behavior causes the burr root to disintegrate instantly and cause delamination of the edge. Mechanical testing carried out at under cryogenic conditions on AZ91-magnesium reinforced with 15% hollow alumina microspheres showed a similar trend with reduced strain to fracture and decreased ductility at subzero test conditions [13]. This phenomenon is observed during cryogenic machining as reported in literature [42]. Wet

machining (AlmagTM oil) provides effective lubrication to reduce tool abrasion and minimize adhesion of magnesium chips. However, a major drawback in wet machining that is observed in this case is that the pressure coolant could cause flushing away of the brittle surface layer. This surface layer is comprised of the deboned and fractured hollow spheres and brittle magnesium surface, as shown in Fig. 4.14 b. Although the majority of the machined surface falls within an average roughness value of 0.5 µm, the flushing effect causes satellite sites of large craters and microsphere pulled out pits on the bore surface of the drilled hole. This aggravates the risk of subsurface damage to propagate beneath the drilled surface. In dry machining, the plasticity of the magnesium matrix is promoted due to heat generated during the shearing process. This allows the magnesium to flow around the hollow ceramic microspheres causing the material to yield under the applied shear load. This weakens the boundary interface between the metal and the ceramic reinforcement. The longitudinal cracks initiate and propagate to cause several locations of defect generation (Fig. 4.14 c). This allows the longitudinal cracks to coalescence with the transverse matrix cracks to constitute the shearing process. The material side due to the plastic flow of the matrix is also enhanced. This causes the material to push out due to the combined effect of thermal and shear load factors acting on the foam material during the drilling process. Thus, the height of burr formation during dry machining is comparably larger than the wet and cryogenic machining.

Fig. 4.15a and 4.15b show the effect of hollow microsphere reinforcement on the entry and exit burr height during dry cutting of AZ91 magnesium syntactic foam. The test results show a decrease in burr height with increasing volume fraction. As the volume fraction rose from 5% to 15%, the entry burr height and exit burr height decreased by 46% and 17%, respectively. Low volume fraction foams recorded an average entry and exit burr height of 63 µm and115 µm, respectively. On the other hand, higher volume fraction foams with 15% vol of hollow alumina recorded average entry and exit burr height of 34 µm and 96 µm, respectively. A decrease in burr height with increasing volume fraction points towards a reduction in ductility of the syntactic foam. This is primarily attributed to an increase in the number of hollow microspheres in the matrix due to an increase in volume fraction for a given average size. The number of defect generation sites is increased. The strain hardening behavior of the magnesium matrix is enhanced due to the Hall-Petch effect of grain boundary pinning by the precipitates and the ceramic hollow spheres. This causes a constraint in the plastic movement of the matrix resulting in the higher hardness of the foam material. The yield

strength of the material is enhanced. The magnesium matrix carries the applied load effectively with lower plastic deformation. Hence the material pushes out phenomenon is reduced in the case of 15% vol foams. With an increasing number of ceramic microspheres, the number of defect generation sites also increases. The rapid coalescence of transverse matrix cracks with longitudinal interfacial cracks promotes the acceleration of crack propagation along a preferential direction and constrains the magnesium material side flow. There is a higher tendency of the brittle cracks to propagate and disintegrate the burr root. This causes delamination of the hole edge at a lower strain value compared to the more ductile low volume fraction foams. This phenomenon is attributed to cause a reduction in burr formation in higher volume fraction magnesium metallic foams.

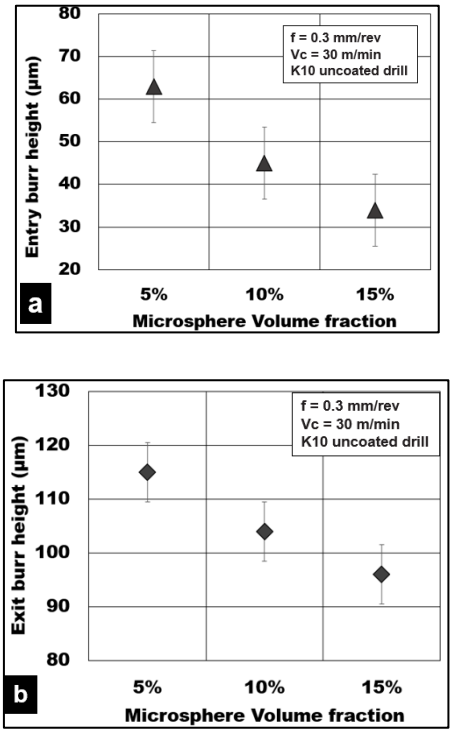


Figure 4. 15 Effect of alumina volume fraction on burr height during machining AZ91-magnesium syntactic foam under dry conditions; (a) Entry burr height and (b) exit burr height.

### 4.5 Chip Morphology

The effect of the lubrication method on the chip morphology during cutting AZ91-15% magnesium syntactic foam is investigated through SEM micrographs (Fig.4.16). The significance of cooling method on the achievable surface integrity during drilling magnesium syntactic foam has been already discussed in the previous section. Application of these novel magnesium syntactic foams in temporary biomedical stents

and implants require excellent surface quality and integrity. The study of chip formation plays an important role in optimizing the drilling process design to achieve the required surface roughness. It has been shown that the surface roughness of the machined implant affects their corrosion behavior [20]. SEM investigation of chip forms shows that the type of chips formed during drilling magnesium foams were primarily discontinuous chips. Chip morphologies during wet and dry cutting of AZ91-15% magnesium foam are shown in Fig.4.16a and 4.16b. As can be seen from the micrographs, the extent of brittle crack initiation and propagation is evident clearly on the tool contact surface of the chips. Chip serrations can be noticed clearly on the chip surface. The spacing between the serrations is approximately between 5-15 μm. After every 3 to 5 small serrations, a brittle matrix crack is evident that splits the chip, causing discontinuity. Past research has shown that the cutting tools used for cutting AZ91 magnesium foams are subjected to both 2-body and 3-body abrasion [12,13]. Wet machining using mineral oil is expected to provide lubrication and reduce the intensity of the abrasion of tool surface by the ceramic microspheres and work-hardened matrix. The generation of high friction is expected to be lower while cutting with wet machining. Adhesion of the magnesium matrix is also expected to be reduced with the usage of mineral oil. With its heat carrying ability induces localized brittle cracking of the matrix with the minimization of heat generation in the cutting zone. It has been discussed in the previous section that the application of mineral oil under pressure is detrimental to surface roughness. Loose, brittle layers get disintegrated, causing a higher percentage of machining induced defects. The coalescence of surface defects is accelerated due to the application of pressure coolant. The cracks run almost along the full length of the chip along the transverse to feed direction. The transverse crack initiation, coalescence, and movement are supported by the presence of voids, pores, and pits present in the matrix in large numbers. Also, micro defects along the boundary region between the matrix and ceramic microspheres promote the longitudinal crack initiation and propagation.

During dry machining, the magnesium plasticity plays an important role in the type of chip formed. The rate of heat dissipation because of the shearing process into the workpiece material is higher during dry cutting. SEM micrographs of chips collected from the dry cutting show a semi-continuous type of chip. A small degree of

edge serrations is noticed. The spacing between these small serrations is approximately the same size as the dry cutting. The transverse crack initiation and propagation to a certain distance is visible. Micrographs show regions of coalescence of transverse and longitudinal cracks. However, there are junctions where the discontinuity in crack coalescence and propagation happens. It is observed that the termination of these cracks has occurred due to the ductility of the magnesium material ahead of the crack leading to the closure of the crack. More matrix ductility has caused material side flow and push out. This results in higher friction and cutting force due to the adhesion of the magnesium matrix in the form of a built-up-edge. A similar chip formation mechanism has been reported in the literature for metal matrix composites [14,43,44].

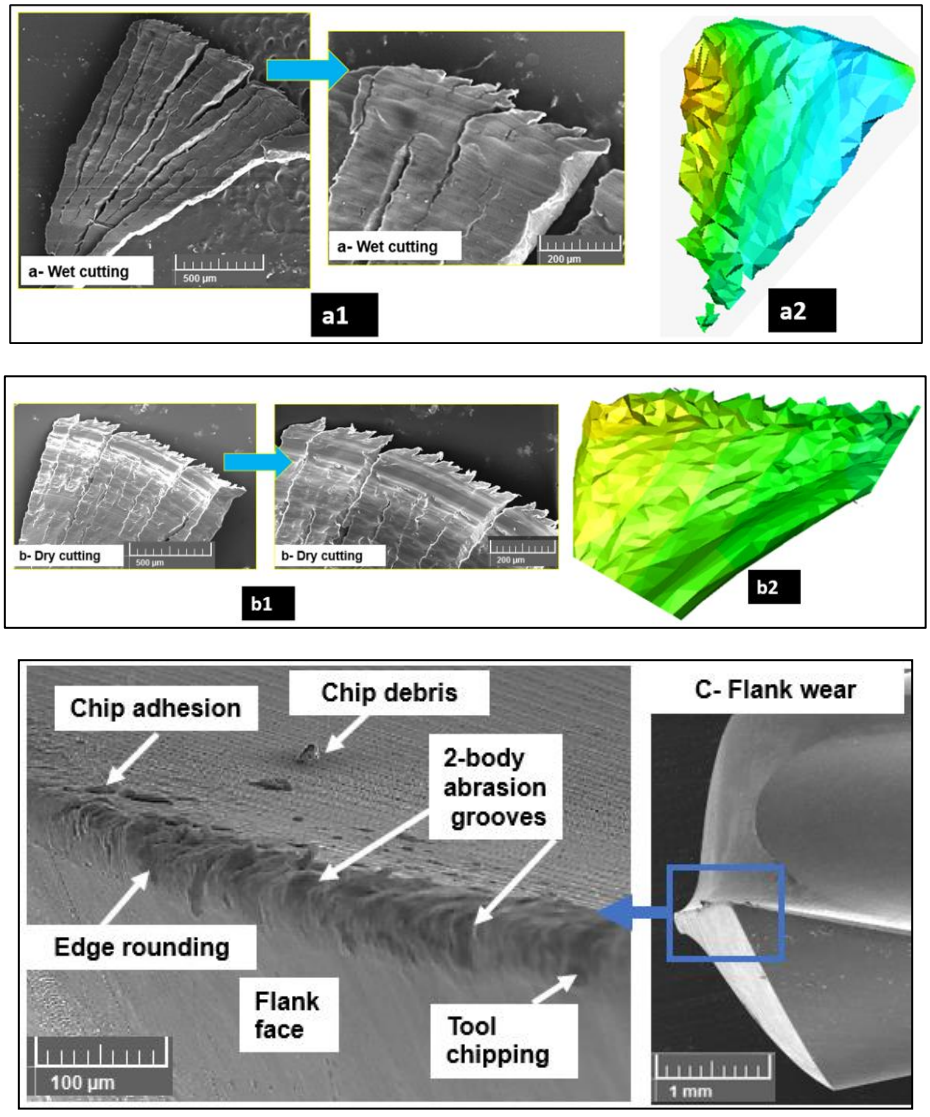


Figure 4. 16 Chip morphology of AZ91-15% magnesium foam a) wet machining b) dry machining c) representative tool wear.

Characteristic tool wear during drilling AZ91 magnesium-15% alumina microsphere syntactic foam is shown in Fig.4.16 c under cryogenic cooling. It is known that the hardness and brittleness of the magnesium foam are increased under cryogenic machining. Investigation of the tool surface shows areas of abrasive wear. Work hardened matrix along with fractured hollow ceramic microspheres engage in both 2-body and 3-body abrasion. Abrasion wear tracks along with chipped edges indicate the brittle behavior of the magnesium syntactic foam while cutting under subzero cooling conditions. As the next step, further tool wear studies will be carried out to characterize the acceleration of tool wear and optimize the tool life during machining AZ91-magnesium syntactic foams.

## 4.6 Damage Mechanics

**4.6.1 Unit cell damage model**. To study the force generated from this novel material through finite element modelling, a unit cell model was investigated to showcase the force relation with one microsphere in the workpiece as shown in Figure 4.17. Table 4.2 shows the parameters for unit cell model.

### 4.6.2 Effect of microsphere size and microsphere wall thickness

Table 4. 2 Unit cell damage model parameters

| Microsphere size mm | Thick -ness | Volume Fraction | Feed per rev (mm/rev) | Feed Rate mm/min | FE Prediction Thrust Force N |
|---|---|---|---|---|---|
| 2 | 0.1 | 15 | 0.2 | 1528.6 | 65 |
| 2 | 0.2 | 15 | 0.2 | 1528.6 | 79 |
| 2 | 0.3 | 15 | 0.2 | 1528.6 | 92 |
| 2.5 | 0.2 | 15 | 0.2 | 1528.6 | 36 |
| 3 | 0.2 | 15 | 0.2 | 1528.6 | 30.6 |

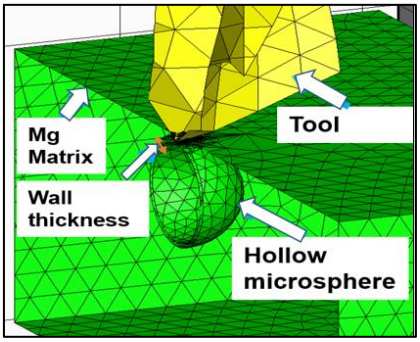


Figure 4. 17 microsphere of 2 mm diameter and 0.1 mm wall thickness

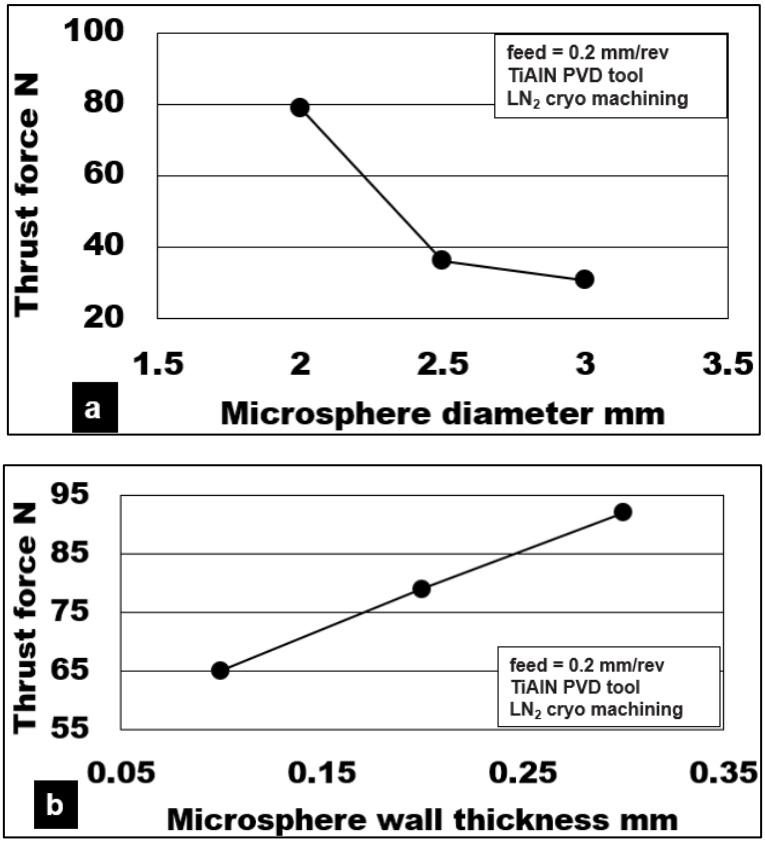


Figure 4. 18 Thrust force variation with a) microsphere diameter and b) microsphere wall thickness.

Microsphere wall thickness and microsphere diameter plays and important role in the investigation of unit cell damage model. Fig 4.18 shows the variation in machining forces generated during drilling AZ91-magnesium syntactic foams reinforced with ceramic microspheres. The cutting test was carried out using TiAlN PVD coated twist drills under cryogenic cooling conditions. The thrust force values show a decrease in values when the diameter of the microsphere increase. A thrust force of 79 N for 2 mm diameter compared to 30 N in case of 3 mm diameter. The microsphere wall thickness effect on the generated thrust forces were addressed in fig. 4.18 b, almost 1.5% increase in thrust force value when the wall thickness is increased from 0.1 mm to 0.3 mm.

## Chapter 5. Conclusions

Machinability studies were carried out on AZ91-magnesium syntactic foams dispersed with hollow aluminum oxide under different lubrication methods. The attainable surface quality & integrity, machining forces, chip morphology, and burr formation were investigated. The following observations were made from this study:

1. During machining AZ91-15% syntactic foams with K10 carbide drill, higher machining forces were generated while cutting under liquid nitrogen cryogenic machining, which was 30%-60% higher than wet and dry machining.
2. During dry machining, higher volume fraction syntactic foams recorded higher machining forces, which increased by almost 200% as the volume fraction increased from 5% to 15%. However, this increase dropped to 50% during cryogenic machining with the increasing volume fraction of hollow alumina.
3. TiAlN PVD coated drills recorded a 20% reduction in machining forces compared to uncoated K10 drills under cryogenic machining AZ91-15% syntactic foam.
4. Under cryogenic drilling with the TiAlN PVD tool, an increasing trend in thrust forces by 233% was recorded from 0.075 mm/rev to 0.6mm/rev. With a further increase in feed rate, the thrust forces showed a decline in magnitude. This is primarily attributed to the onset of thermal softening during drilling AZ91-15% foam.
5. SEM analysis showed that the percentage of drilling-induced sub-surface damages could be minimized through cryogenic machining. Surface finish (Ra) showed a 45%-55% improvement compared to dry and wet machining.
6. Surface roughness (Ra) worsened by 70%-90% while cutting higher volume fraction (15%) syntactic foams under both cryogenic and dry machining conditions.
7. Cryogenic machining showed compression stress behavior compared to wet and dry machining in case of machining induced stresses.
8. Damage model indicated that microsphere diameter increase will decrease the drilling thrust force by 50%, while microsphere wall thickness will increase its value by 40%.
9. In conclusion, cryogenic machining is recommended for drilling AZ91 magnesium syntactic foams using the TiAlN PVD tool.

## References


[1] R. Reddy Nagavally, “Composite materials-history, types, fabrication techniques, advantages, and applications,” *Int. J. Mech. Prod. Eng.*, vol 1-5, no. 5, pp. 2320–2092, 2017.

[2] K. K. Chawla, *Composite materials: Science and engineering, third edition.* Springer, New York, 2012, pp. 1-542.

[3] S. Kannan and H. A. Kishawy, “Tribological aspects of machining aluminium metal matrix composites,” *J. Mater. Process. Tech.*, vol. 1–3, no. 198, pp. 399–406, Mar. 2008, doi: 10.1016/J.JMATPROTEC.2007.07.021.

[4] H. Z. Ye and X. Y. Liu, “Review of recent studies in magnesium matrix composites,” *J. Mater. Sci. 2004 3920*, vol. 39, no. 20, pp. 6153–6171, Oct. 2004, doi: 10.1023/B:JMSC.0000043583.47148.31.

[5] Sarapure, B. Satish, B. Girish and Basawaraj, "Microstructure and Mechanical Behavior of Magnesium Alloy AZ91 Hybrid Composites", IOP Conference Series: Materials Science and Engineering, vol. 310, p. 012161, 2018. Available: 10.1088/1757-899x/310/1/012161.

[6] R. I. Rubel and S. S. Yusuf, “A review on syntactic foams processing, preparation and applications,” in *Proc. ICMERE,* 2019, pp. 117–123.

[7] S. Sankaran, B. N. Ravishankar, K. Ravi Sekhar, S. Dasgupta, and M. N. Jagdish Kumar, “Syntactic foams for multifunctional applications,” *Compos. Mater. Process. Appl. Charact.*,vol 65, no 6, pp. 281–314, Jan. 2016, doi: 10.1007/978-3-662-49514-8_9.

[8] P. K. Rohatgi, N. Gupta, B. F. Schultz, and D. D. Luong, “The synthesis, compressive properties, and applications of metal matrix syntactic foams,” *JOM 2011 632*, vol. 63, no. 2, pp. 36–42, Feb. 2011, doi: 10.1007/S11837-011-0026-1.

[9] G. Parande, V. Manakari, G. K. Meenashisundaram, and M. Gupta, “Enhancing the hardness/compression/damping response of magnesium by reinforcing with biocompatible silica nanoparticulates,” *Int. J. Mater. Res.*, vol. 107, no. 12, pp. 1091–1099, Dec. 2016, doi: 10.3139/146.111435.

[10] G. Cao, H. Konishi, and X. Li, “Mechanical properties and microstructure of Mg/SiC nanocomposites fabricated by ultrasonic cavitation based

nanomanufacturing," *J. Manuf. Sci. Eng. Trans. ASME*, vol. 130, no. 3, pp. 0311051–0311056, 2008, doi: 10.1115/1.2823086.

[11] K. Kumar, R. S. Gill, and U. Batra, "Challenges and opportunities for biodegradable magnesium alloy implants," *Mater. Technol.*, vol. 33, no. 2, pp. 153–172, 2018, doi: 10.1080/10667857.2017.1377973.

[12] S. Kannan, S. Pervaiz, A. Alhourani, R. Klassen, R. Selvam and M. Haghshenas, "On the Role of Hollow Aluminium Oxide Microballoons during Machining of AZ31 Magnesium Syntactic Foam", *Materials*, vol. 13, no. 16, p. 3534, 2020. Available: 10.3390/ma13163534.

[13] S. Kannan, S. Pervaiz, R. J. Klassen, D. Huo, and M. Haghshenas, "An energy-based analysis for machining novel AZ91 magnesium composite foam dispersed with ceramic microspheres," *J. Manuf. Sci. Eng. Trans. ASME*, vol. 143, no. 3, pp. 1–10, 2021, doi: 10.1115/1.4048438.

[14] B. Davis, D. Dabrow, L. Ju, A. Li, C. Xu, and Y. Huang, "Study of Chip Morphology and Chip Formation Mechanism during Machining of Magnesium-Based Metal Matrix Composites," in *Proc. MSEC,* 2017, pp. 3043-3052.

[15] Z. G. Wang *et al.*, "Study on orthogonal turning of titanium alloys with different coolant supply strategies," *Int. J. Adv. Manuf. Technol. 2008 427*, vol. 42, no. 7, pp. 621–632, Jul. 2008, doi: 10.1007/S00170-008-1627-X.

[16] H. Wang, Y. Estrin, H. Fu, G. Song, and Z. Zúberová, "The Effect of Pre-Processing and Grain Structure on the Bio-Corrosion and Fatigue Resistance of Magnesium Alloy AZ31," *Adv. Eng. Mater.*, vol. 9, no. 11, pp. 967–972, Nov. 2007, doi: 10.1002/ADEM.200700200.

[17] Z. Pu *et al.*, "Grain refined and basal textured surface produced by burnishing for improved corrosion performance of AZ31B Mg alloy," *Corros. Sci.*, vol. 57, pp. 192–201, Apr. 2012, doi: 10.1016/J.CORSCI.2011.12.018.

[18] J. C. Outeiro, F. Rossi, G. Fromentin, G. Poulachon, G. Germain, and A. C. Batista, "Process Mechanics and Surface Integrity Induced by Dry and Cryogenic Machining of AZ31B-O Magnesium Alloy," *Procedia CIRP*, vol. 8, pp. 487–492, Jan. 2013, doi: 10.1016/J.PROCIR.2013.06.138.

[19] Z. Pu, J. C. Outeiro, A. C. Batista, O. W. Dillon, D. A. Puleo, and I. S. Jawahir, "Enhanced surface integrity of AZ31B Mg alloy by cryogenic machining

towards improved functional performance of machined components," *Int. J. Mach. Tools Manuf.*, vol. 56, pp. 17–27, May 2012, doi: 10.1016/J.IJMACHTOOLS.2011.12.006.

[20] Z. Pu, D. Umbrello, O. W. Dillon, T. Lu, D. A. Puleo, and I. S. Jawahir, "Technical Paper," *J. Manuf. Process.*, vol. 2, no. 16, pp. 335–343, 2014, doi: 10.1016/J.JMAPRO.2014.02.002.

[21] U. Koklu and H. Coban, "Effect of dipped cryogenic approach on thrust force, temperature, tool wear and chip formation in drilling of AZ31 magnesium alloy," *J. Mater. Res. Technol.*, vol. 9, no. 3, pp. 2870–2880, May 2020, doi: 10.1016/J.JMRT.2020.01.038.

[22] M. Saravanakumar, N. Nanjappan, and K. Vijayan, "Study of cutting forces in machining of magnesium composite by response surface methodology," *Carbon - Sci. Technol.*, vol. 7, pp. 36–58, Jan. 2015.

[23] X. Teng, D. Huo, E. Wong, G. Meenashisundaram, and M. Gupta, "Micro-machinability of nanoparticle-reinforced Mg-based MMCs: an experimental investigation," *Int. J. Adv. Manuf. Technol. 2016 875*, vol. 87, no. 5, pp. 2165–2178, Mar. 2016, doi: 10.1007/S00170-016-8611-7.

[24] F. Sun, D. Huo, G. Fu, X. Teng, S. Kannan, and H. Zhang, "Micro-drilling of Mg-based MMCs reinforced with SiO2 nanoparticles: An experimental approach:," *https://doi.org/10.1177/0954405420929784*, vol. 234, no. 12, pp. 1473–1485, Jun. 2020, doi: 10.1177/0954405420929784.

[25] A. H. Kheireddine, A. H. Ammouri, T. Lu, O. W. Dillon, R. F. Hamade, and I. S. Jawahir, "An experimental and numerical study of the effect of cryogenic cooling on the surface integrity of drilled holes in AZ31B Mg alloy," *Int. J. Adv. Manuf. Technol. 2014 781*, vol. 78, no. 1, pp. 269–279, Dec. 2014, doi: 10.1007/S00170-014-6650-5.

[26] A. H. Kheireddine, A. H. Ammouri, T. Lu, I. S. Jawahir, and R. F. Hamade, "An FEM Analysis with Experimental Validation to Study the Hardness of In-Process Cryogenically Cooled Drilled Holes in Mg AZ31b," *Procedia CIRP*, vol. 8, pp. 588–593, Jan. 2013, doi: 10.1016/J.PROCIR.2013.06.156.

[27] S. Bhowmick, M. J. Lukitsch, and A. T. Alpas, "Dry and minimum quantity lubrication drilling of cast magnesium alloy (AM60)," *Int. J. Mach. Tools*

*Manuf.*, vol. 50, no. 5, pp. 444–457, May 2010, doi: 10.1016/J.IJMACHTOOLS.2010.02.001.

[28] F. Berzosa, B. De Agustina, and E. M. Rubio, "Tool Selection in Drilling of Magnesium UNSM11917 Pieces under Dry and MQL Conditions Based on Surface Roughness," *Procedia Eng.*, vol. 184, pp. 117–127, Jan. 2017, doi: 10.1016/J.PROENG.2017.04.076.

[29] B. De Agustina, F. Berzosa, E. M. Rubio, and M. M. Marín, "Experimental study of magnesium drilling based on the surface quality," *Procedia CIRP*, vol. 79, pp. 74–78, 2019, doi: 10.1016/J.PROCIR.2019.02.014.

[30] M. Arai, S. Sato, M. Ogawa, and H. Shikata, "Chip control in finish cutting of magnesium alloy," *J. Mater. Process. Technol.*, vol. 62, no. 4, pp. 341–344, Dec. 1996, doi: 10.1016/S0924-0136(96)02432-6.

[31] N. Tomac, K. Tonnessen, and F. O. Rasch, "Formation of Flank Build-up in Cutting Magnesium Alloys," *CIRP Ann.*, vol. 40, no. 1, pp. 79–82, Jan. 1991, doi: 10.1016/S0007-8506(07)61938-6.

[32] J. Wang, Y. B. Liu, J. An, and L. M. Wang, "Wear mechanism map of uncoated HSS tools during drilling die-cast magnesium alloy," *Wear*, vol. 265, no. 5–6, pp. 685–691, Aug. 2008, doi: 10.1016/J.WEAR.2007.12.009.

[33] S. Bhowmick and A. T. Alpas, "The role of diamond-like carbon coated drills on minimum quantity lubrication drilling of magnesium alloys," *Surf. Coatings Technol.*, vol. 205, no. 23–24, pp. 5302–5311, Sep. 2011, doi: 10.1016/J.SURFCOAT.2011.05.037.

[34] S. Chen, D. Head, M. Effgen, and I. S. Jawahir, "An investigation of sustained machining performance for controlled surface quality requirements in porous tungsten," *IEEE Trans. Electron Devices*, vol. 52, no. 5, pp. 903–908, May 2005, doi: 10.1109/TED.2005.846352.

[35] J. Schoop, M. Effgen, T. J. Balk, and I. S. Jawahir, "Improved Product Quality and Resource Efficiency in Porous Tungsten Machining for Dispenser Cathode Application by Elimination of the Infiltration Process," *Re-Engineering Manuf. Sustain. - Proc. 20th CIRP Int. Conf. Life Cycle Eng.*, pp. 241–244, 2013, doi: 10.1007/978-981-4451-48-2_39.

[36] M. Heidari and J. Yan, "Ultraprecision surface flattening of porous silicon by

diamond turning," *Precis. Eng.*, vol. 49, pp. 262–277, Jul. 2017, doi: 10.1016/J.PRECISIONENG.2017.02.015.

[37] F. Pusavec, "Porous tungsten machining under cryogenic conditions," *Int. J. Refract. Met. Hard Mater.*, vol. 35, pp. 84–89, Nov. 2012, doi: 10.1016/J.IJRMHM.2012.04.009.

[38] Z. Trojanova and P. Lukac. *Hardening and Softening in Magnesium Alloys* Rijeka,Croatia: InTech, 2011, pp. 1-526.

[39] "ChevronTexacoAlmag® Oil." http://www.matweb.com/search/datasheettext.aspx?matguid=16e5120cdaea4aa8a9de98e8c06c244d (accessed Aug. 06, 2021).

[40] J. Deng, F. Wu, Y. Lian, Y. Xing, and S. Li, "Erosion wear of CrN, TiN, CrAlN, and TiAlN PVD nitride coatings," *Int. J. Refract. Met. Hard Mater.*, vol. 35, pp. 10–16, Nov. 2012, doi: 10.1016/J.IJRMHM.2012.03.002.

[41] S. Y. Hong, Y. Ding, and W.-C. Jeong, "Friction and cutting forces in cryogenic machining of Ti-6Al-4V," *Int. J. Mach. Tools Manuf.*, vol. 41, pp. 2271–2285, 2001, Accessed: Aug. 06, 2021. [Online]. Available: http://www.paper.edu.cn.

[42] S. S. Joshi, N. Ramakrishnan, and P. Ramakrishnan, "Microstructural analysis of chip formation during orthogonal machining of Al/SiCp compo," *J. Eng. Mater. Technol. Trans. ASME*, vol. 123, no. 3, pp. 315–321, Jul. 2001, doi: 10.1115/1.1356026.

[43] H. Zhang, X. Kong, L. Yang, Y. Wang, and G. Chi, "High temperature deformation mechanisms and constitutive modeling for Al/SiCp/45 metal matrix composites undergoing laser-assisted machining," *Mater. Sci. Eng. A*, vol. 642, pp. 330–339, Aug. 2015, doi: 10.1016/J.MSEA.2015.06.052.

[44] M. Murugesan and D. W. Jung, "Johnson cook material and failure model parameters estimation of AISI-1045 medium carbon steel for metal forming applications,"*Materials (Basel).*, vol. 12, pp. 609-627, 2019, doi: 10.3390/ma12040609.

[45] K. Bobzin, M. Öte, S. Wiesner, L. Gerdt, A. Bührig-Polaczek, and J. Brachmann, "Effect of Alloying Elements on Growth Behavior of Intermetallic Compounds at the Cold-Sprayed Coating/Steel Interface During Immersion in Aluminum Melt," *Int. J. Met.*, vol. 12, no. 4, pp. 712–721, Oct. 2018, doi: 10.1007/S40962-

017-0205-0.

[46] K. Bobzin *et al.*, “Comparison of Residual Stress Measurements Conducted by X-ray Stress Analysis and Incremental Hole Drilling Method,” *J. Therm. Spray Technol.*, vol. 29, no. 6, pp. 1218–1228, Aug. 2020, doi: 10.1007/S11666-020-01056-Z.

[47] M. Peron, R. Bertolini, A. Ghiotti, J. Torgersen, S. Bruschi, and F. Berto, “Enhancement of stress corrosion cracking of AZ31 magnesium alloy in simulated body fluid thanks to cryogenic machining,” *J. Mech. Behav. Biomed. Mater.*, vol. 101, p. 103429, Jan. 2020, doi: 10.1016/J.JMBBM.2019.103429.

[48] I. Zagórski and J. Korpysa, “Surface quality assessment after milling AZ91D magnesium alloy using PCD tool,” *Materials (Basel).*, vol. 13, pp. 617-637, Feb. 2020, doi: 10.3390/MA13030617.

## Vita

Abdalla Mohammed was born in 1994, in Khartoum, in Sudan. He was educated in local public schools and graduated from Khartoum University in 2016.His degree was a Bachelor of Science in Mechanical Engineering.

In September 2018, he joined the Mechanical Engineering master's program at the American University of Sharjah as a graduate student.

Mr. Abdalla is a member of the Institution of Mechanical Engineers, IMechE. His research interest is in drilling and simulation of syntactic foams.